Aus der Klinik für Diagnostische und Interventionelle Radiologie

Universitätsklinikum des Saarlandes, Homburg/Saar

(Direktor: Prof. Dr. Arno Bücker)

Evaluation of liver tumor perfusion by intraarterial transcatheter magnetic resonance angiography during transarterial chemoembolization in patients with hepatocellular carcinoma: Preclinical instrument validation in vascular models and clinical study

Dissertation zur Erlangung des Grades eines Doktors der Medizin

der Medizinischen Fakultät

der UNIVERSITÄT DES SAARLANDES

2013

vorgelegt von: Malgorzata Wolska-Krawczyk

geb. am: 04.05.1982 in Lublin, Polen

Abbreviations

2D	Two-dimensional
3D	Three-dimensional
ASTM	American Society for Testing and Materials
BCLC	Barcelona Clinic Liver Cancer
bSSFP	Balanced steady state free precession
C	Celsius
CCC	Cholangiocellular carcinoma
CE	European Conformity
CNR	Contrast to noise ratio
CT	Computed tomography
DSA	Digital subtraction angiography
EASL	European Association for the Study of the Liver
ECOG	Eastern Cooperative Oncology Group
EPI	Echoplanar imaging
F	French
FA	Flip angle
FLASH	Fast low angle shot
FOV	Field of view
Gd	Gadolinium
Gd-BOPTA	Gadolinium-gadobenate dimeglumin
Gd-DOTA	Gadolinium- 1,4,7,10-tetraazacyclododecane-1,4,7,10- tetraacetic acid
GE	Gradient echo
GRAPPA	Generalized Autocalibrating Partially Parallel Acquisition
GW	Guidewire
GWs	Guidewires
Gy	Gray

HBV	Hepatitis B virus
HCC	Hepatocellular carcinoma
HCV	Hepatits C virus
i.a.	Intraarterial
IIIOS	Integrated Interventional Imaging Operating System
iMRI	Interventional magnetic resonance imaging
IMSaT	Institute of Medical Science and Technology
ISO	International Organization of Standardization
i.v.	Intravenous
l	Liter
MHz	Megahertz
Min	Minute
MR	Magnetic resonance
MRI	Magnetic resonance imaging
NASH	Nonalcoholic steatohepatits
PEEK	Polyetheretherketone
RF	Radiofrequency
RFA	Radiofrequency ablation
ROI	Region of interests
s	Second
SAR	Specific absorption rate
SD	Standard deviation
SE	Spin echo
SI	Signal intensity
SIRT	Selective internal radiation therapy
SNR	Signal to noise ratio
SPGR	Spoiled gradient echo

SSFP	Steady state free precession
ST	Slice thickness
Sv	Sievert
T	Tesla
TACE	Transarterial chemoembolization
TAE	Transarterial embolization
TE	Time to echo
TIPS	Transjugular intrahepatic portosystemic shunt
TR	Time of repetition
TSE	Turbo spin echo
VIBE	Volumetric interpolated breath hold

I. ZUSAMMENFASSUNG

Hintergrund

Magnetresonanztomographie (MR)-gesteuerte endovaskuläre Interventionen bieten aufgrund des Fehlens ionisierender Strahlung, der Möglichkeit einer dreidimensionalen (3D) Bildakquisition und eines ausgezeichneten Weichteilkontrasts, zahlreiche Vorteile gegenüber der konventionellen Röntgenfluoroskopie. Das aktuell größte Hindernis bei der Durchführung endovaskulärer MR Interventionen ist der Mangel an geeigneten Instrumenten. Kommerziell erhältliche metallische Führungsdrähte und Katheter sind aufgrund ihrer Leitfähigkeit im MR Feld und ihrer potentiellen Radiofrequenz (RF) Erhitzung als MR-unsicher einzustufen. In der präklinischen Phase unserer Studie (Teil 1) wurden daher verschiedene interventionelle Instrumente an drei vaskulären Phantomen in einem 1,5 Tesla (T) MR Feld evaluiert zwecks der zukünftigen Anwendung zur intraarteriellen (i.a.) transkatheter MR-Angiographie während einer transarteriellen Chemoembolisation (TACE) (Teil 2). Eine anatomisch unerwartete arterielle Tumorversorgung kann im Rahmen einer TACE zur fehlgeleiteten Chemotherapie und unzureichender Behandlung des Tumors führen. Ziel der Studie war die Evaluation der zusätzlich zur TACE durchgeführten i.a. MR-Angiographie im Hinblick auf einen diagnostischen und auch therapeutischen Gewinn.

Material und Methoden

Teil 1: Das Auftreten von Suszeptibilitätsartefakten in drei Gradientenechosequenzen (GE) und einer Turbo-Spin-Echo-Sequenz wurde für 13 Katheter an zwei verschiedenen vaskulären Modellen ausgewertet. Zudem wurden zwei MR-kompatible Prototypen von Führungsdrähten auf Suszeptibilitätsartefakte und RF-Erhitzung in vaskulären Modellen sowie in menschlichen Kadavern getestet. Die als MR-tauglich eingestuften Instrumente wurden im Rahmen des klinischen Teils der Studie angewendet.

Teil 2: Bei 27 Patienten wurden 62 TACE mit i.a. transkatheter MR-Angiographie kombiniert durchgeführt. Zunächst wurde der Katheter unter Fluoroskopiekontrolle in die Tumor

versorgende Arterie gesteuert. Kontrastgestützte i.a. transkatheter MR-Angiographie (10 ml Gadolinium-DOTA 5.0% Dotarem, Guerbet, Frankreich) wurde in der arteriellen, portalvenösen und spätvenösen Phase durchgeführt. Hierfür wurden zwei GE Sequenzen (FLASH 3D, VIBE, Siemens Magnetom Aera 1,5T) eingesetzt um die Tumorperfusion zu evaluieren. Die Bilder wurden qualitativ durch zwei Radiologen ausgewertet. Die quantitative Auswertung erfolgte über die „region of interest" (ROI) Analyse. Signal- und Kontrast-Rausch-Verhältnis (SNR- und CNR) für FLASH 3D und VIBE Sequenzen wurden mit dem Mann-Whitney-Test verglichen.

Ergebnisse

Teil 1: Gleitbeschichtete 4 und 5 French (F) Katheter (Terumo, Tokio, Japan) verursachten keine Artefakte in den gewählten Sequenzen und wurden während des klinischen Teils der Studie benutzt. MR-kompatible Führungsdrähte waren zum Zeitpunkt der Experimente in der präklinischen Phase noch nicht zur Verwendung am Menschen zugelassen.

Teil 2: Die i.a. transkatheter MR-Angiographie bestätigte die korrekte Katheterpositionierung in 53/62 (85%) Interventionen und führte zur Katheterrepositionierung in drei Fällen. Eine zusätzliche arterielle Tumorversorgung wurde in sechs Fällen nachgewiesen. Neue Herde wurden in vier Fällen identifiziert. Die quantitative Analyse der SNR im Tumor ergab eine Überlegenheit der VIBE Sequenz (arterielle Phase: Median 36,96 [Minimum 9,92 - Maximum 91,54], portalvenöse Phase: 28,59 [10,48 - 83,89], spätvenöse Phase: 24,37 [10,21 - 72,28]) gegenüber der FLASH 3D Sequenz (arterielle Phase: 21,36 [7,79 - 50,11], portalvenöse Phase: 20,25 [5,50 - 57,87], spätvenöse Phase: 16,19 [5,83 - 51,03], p-Werte: 0,02, 0,01 und 0,002). Der Vergleich der CNR ergab keine signifikanten Unterschiede (alle $p > 0,05$).

Schlussfolgerung

Gleitbeschichtete Katheter (Terumo, Tokyo, Japan) sind in der von uns genutzten MR-Umgebung MR-kompatibel und sind als sicher während endovaskulärer Verfahren

einzustufen. Die i.a. transkatheter MR-Angiographie bei TACE ermöglicht die Visualisierung der Kathetersposition und hilft eine fehlerhafte oder unzureichende Tumorembolisation zu verhindern. Die VIBE Sequenz erzielt eine höhere SNR aber keine verbesserte CNR verglichen mit der FLASH 3D Sequenz.

II. ABSTRACT

Background

Endovascular interventions in magnetic resonance (MR) offer potential benefits like lack of ionizing radiation, three-dimensional (3D) imaging or soft tissue contrast, compared to other techniques. The main hurdle in performing MR interventions is the lack of appropriate devices. Regular guidewires (GWs) and catheters cause conductivity and potential radiofrequency (RF) heating due to their metallic components. Consequently, they are considered MR unsafe. In the preclinical phase of the study (part 1) we evaluated potentially MR compatible interventional devices in vascular phantoms at 1.5 Tesla (T). Our aim was to study their future application during transarterial chemoembolization (TACE) complemented with intraarterial (i.a.) transcatheter MR angiography (part 2). The usefulness of i.a. transcatheter MR angiography during TACE was evaluated.

Materials und Methods

Part 1: Several experiments with 13 catheters on two different vasculars models were conducted. The occurrence of susceptibility artifacts was evaluated in three gradient echo (GE) sequences and one turbo spin echo (TSE) sequence. MR compatible prototypes of GWs were tested for artifact size and RF heating in vascular models as well as in human cadaver. Devices qualified as MR compatible were used during the clinical part of the study. Part 2: Overall, 27 patients with hepatocellular carcinoma (HCC) underwent 62 TACE procedures combined with i.a. transcatheter MR angiography. Prior to embolization a catheter was guided by X-ray fluoroscopy into the HCC supplying artery. Contrast-enhanced i.a. transcatheter MR angiography (10 ml Gadolinium-DOTA 5.0% Dotarem, Guerbet, France) was performed in arterial, portalvenous and late venous phase using either three-dimensional fast low angle shot (FLASH 3D) or volume interpolated breath hold (VIBE) sequences (Siemens Magnetom Aera 1.5T) to study tumor perfusion. The images were evaluated qualitatively by two radiologists. Quantitative evaluation was performed using the

region of interest (ROI) analysis. Signal and contrast to noise ratios (SNR and CNR) for FLASH 3D and VIBE sequences were compared by Mann-Whitney test.

Results

Part 1: Several 4 and 5 French (F) catheters with hydrophilic coating (Terumo, Tokyo, Japan) caused no artifacts in applied sequences and were employed during the clinical part of the study. MR compatible GWs were by the time of our experiments in the preclinical phase of research and their use in patients was not permitted.

Part 2: I.a. transcatheter MR angiography confirmed correct catheter positioning in 53/62 (85%) procedures. Additional collateral tumor vascularization was detected in six cases. New lesions were identified in four patients during this procedure. Quantitative analysis of SNR in tumor demonstrated that the VIBE sequence (arterial: median 36.96 [range: 9.92 - 91.54], portalvenous: 28.59 [10.48 - 83.89] and late venous: 24.37 [10.21 - 72.28]) is superior to the FLASH 3D (arterial: 21.36 [7.79 - 50.11], portalvenous: 20.25 [5.50 - 57.87] and late venous phase: 16.19 [5.83 - 51.03], p values: 0.02, 0.01 and 0.002 respectively). The comparison of CNR yielded no significant differences (all $p > 0.05$).

Conclusion

Catheters with hydrophilic coating are safe when used at 1.5 T MR field during endovascular procedures. I.a. transcatheter MR angiography during TACE enables visualization of the catheter position and may prevent erroneous/insufficient tumor embolization. VIBE-sequence achieves a superior SNR but not CNR as compared to FLASH 3D.

III. INTRODUCTION

III.1 Vascular interventions and imaging in MR

Interventional radiology is a rapidly expanding field due to its minimal invasiveness. Apart from biopsies or drainages, endovascular techniques are especially successful. Stenotic or occluded vessels, bleedings, vessels malformations or tumors can be treated under X-ray guidance. Since these interventions require X-ray guidance (fluoroscopy or CT-guidance), they trigger discussions about potential risks of ionizing radiation exposure. Indeed, a retrospective study published recently in Lancet (59) shows a clear association between exposure to a high radiation dose in childhood and increased occurrence of leukemia or brain cancer in the maturity. In this study the authors analyzed 283.919 CT scans in children under 15 years old and demonstrated that cumulative ionizing radiation of ~50 miligrey (mGy) (5-10 CT body scans) triples the occurrence of leukemia while dosage of ~60 mGy (2-3 CT head scans) can triple the occurrence of brain tumors in adulthood (59). The radiation doses during fluoroscopy depend on procedure length and may vary from 4.0 milisievert (mSv) in simple biliary drainage up to 49.5 mSv in more complicated transjugular intrahepatic portosystemic shunt (TIPS) (16). As a matter of principle, radiation exposure of the patient should be kept to minimum and if possible other imaging methods should be preferred. Brenner et al. (7) stated that the potential risk of inducing cancer due to ionizing radiation varies and depends on life expectancy of the individual. Hence, radiation exposure to physicians regularly performing interventions should be kept to a minimum. The mean natural radiation dose for a human being is 2.4 mSv per year (19) and additional radiation dose has to be strictly monitored. Another issue in fluoroscopy guided procedures is the need for contrast media, that if applied in high doses, especially in patient with impaired renal function (58), may lead to contrast induced nephropathies (3, 53). Considering the above-mentioned drawbacks, magnetic resonance imaging (MRI) has the potential to overcome most of these problems.

MRI is a relatively novel technique that provides anatomical and functional information superior to fluoroscopy and to CT. The discovery of MR is related to the Nobel Prize awarded in 1952 to Felix Bloch and Edward Purcell, who independently discovered the MR phenomenon in 1946. The first prerequisites were established much earlier: the mathematical transformation needed for MRI was discovered by the Napoleon's chief engineer, Jean Baptiste Joseph Fourier, in the 19th century. Nevertheless, the possibility of exploitation of magnetic resonance in imaging appeared for the first time in 1960 when the first MR scanner prototypes were built. Paul Lauterbur, a chemistry professor at the University of New York, set the foundation for MR imaging by performing an image formation on small tube samples in MR and introduced the use of gradients in the static magnetic field. Terms like slice selection, active magnetic shielding, gradient coils or echo planar imaging (EPI) were developed by Sir Peter Mansfield in the late 70's. Eventually the noninvasive MR imaging method of human internal tissues was possible and P. Lauterbur together with Sir P. Mansfield received in 2003 the Nobel Prize for their work. Although MRI has undergone many advances over the past years, the basic principle remains the same. Briefly, this technique is based on resonant effects of protons of hydrogen atoms that build up to 80% of the human body. Energy that is emitted by the MR scanner in form of radio waves interacts with the protons of hydrogen nuclei. Receiver coils deliver the signal that is subsequently transformed by a computer system and used to produce the detailed images of the human body. Specific sequences of RF pulses and switching of the gradients define the signal magnitude. Investigations in the field of MRI were performed in the 80's and 90's of the last century however the topic of interventional MRI (iMRI) is still emerging. Not only lack of ionizing radiation but also possibility to delineate between diseased and healthy tissue, 3D imaging, excellent soft tissue contrast, multiplanar scan capabilities as well as use of non-iodized contrast agents in low doses make MRI a desirable technique in guidance of interventional radiology. To date biopsies and drainages under MR guidance are well-established procedures. MR guidance of endovascular procedures is more demanding and is

still a challenge in clinical MR application. To date, numerous investigations have demonstrated the feasibility of endovascular stenting (11,28), balloon angioplasty (12), vena cava filter placement (43) or heart valve implantation (38) in animal trials. Lack of MR compatible and simultaneously safe devices remains the largest hurdle for clinical investigations. Indeed, conventional guidewires (GWs) or catheters are not MR safe and generate eddy currents due to conductivity of their metallic components. Currently available implants, on the other hand, although not always hazardous, induce distortions of the magnetic field that renders their localization on MR images impossible. On this account, several business concerns have developed MR compatible and safe devices; the prototypes are by now available for clinical research.

III.2 Interventional MR scanners

The MR scanner consists of a magnet that creates a static magnetic field. Radiofrequency transmitter produces and receiver coils register the signal. Magnetic field gradients are applied to localize the signal. The scanners dedicated to interventional MRI were developed in the first half of 1990 and differ substantially from regular ones. These specific scanners have to fulfill the need of facilitated patient access. The first dedicated system, which was introduced in 1994, was characterized by a vertical gap between two magnets termed "double doughnut" (66). The operator could stand between two halves of the magnet and this way perform interventions with his hand on the patient who was placed in the isocenter of the MR field. Some tradeoffs however restricted utility of these scanners. For example, the 58 cm gap between the magnets was too tight for some surgeons, the 0.5 T field strength ranged in the midfield sector with reduced imaging capabilities compared to 1.5 T high field magnets. Moreover, most of the surgical and anesthetic instruments were not even MR compatible and most certainly not MR safe at that time. Therefore low safety of the procedures, difficult cooperation between anesthesia, surgery and radiology teams confined the practicability and profitability of these early devices. Current interventional MR scanners focus more on advancing the MR sequences dedicated to MR guided procedures than on patient's access. Our institution (Clinic of diagnostic and interventional radiology, Homburg, Germany) is equipped with an MR scanner with 1.5 T (Magnetom Aera, Siemens, Erlangen, Germany) with 70 cm wide MR bore; this scanner is in close proximity to an angiography suite with just 3.7 meter in between both rooms (**Figure 1**).
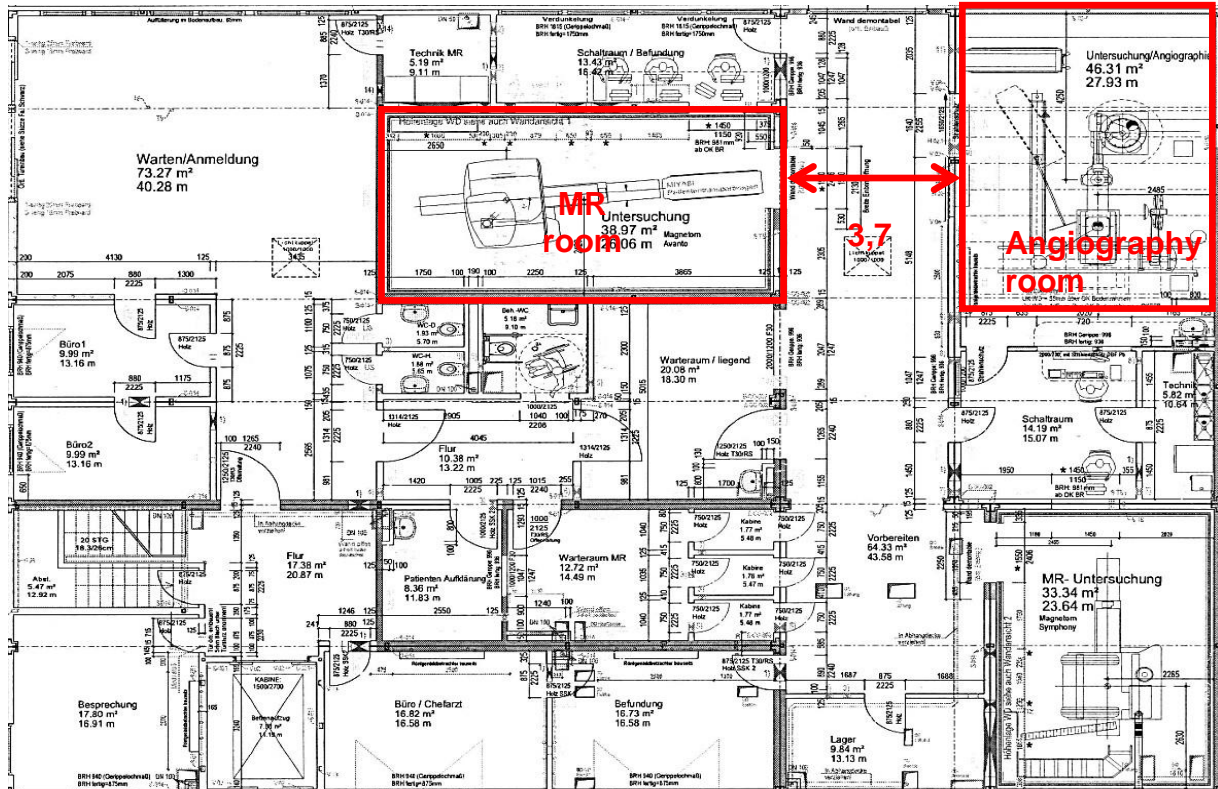
Figure 1

Layout of the 1.5 T MR scanner used for vascular interventions in close proximity to an angiography suite in the Clinic of Diagnostic and Interventional Radiology, Saarland Medical Center, Homburg, Germany.

III.3 MRI Sequences in interventional procedures

The strategy of acquiring MR images during the interventional procedures differs from the one used in the diagnostic MRI. In particular, image acquisition time has to be much shorter to allow steering of interventional instruments (63). Visualization of interventional devices and anatomy with a frame rate of approximately ten images per second without losing image quality is the most crucial feature. However, due to the physics of MRI the increase of imaging speed is accompanied by loss of spatial resolution. Sequences like steady state free precession (SSFP) or fast low angle shot (FLASH) are most often in use for MR guided interventions. In currently available MR scanners, SSFP image with a matrix of 128 x 128 mm can be achieved in approximately 0.4 second (65). Moreover, this technique allows the delineation of blood vessels without application of contrast agent (65). FLASH allows a rapid acquisition of T1 weighted images and if applied after injection of T1 shortening contrast agent offers vessel accentuation in MR angiography (32). Current interventional MR scanners offer the opportunity to manipulate scan parameters inside the scanner room and to observe the images on an in-room monitor. Sequences applied for angiography examinations in our institution were by the time of the study: three-dimensional FLASH (FLASH 3D) and volumetric interpolated breath hold (VIBE) sequences. The latter one a modified FLASH 3D sequence with the advantage of depicting soft tissue around the vessel and not the vessel only.

III.3.1 Signal to noise ratio (SNR) and contrast to noise ratio (CNR)

Signal to noise ratio (SNR) is a commonly used parameter to investigate the quality of MR images (36). In brief, the signal is measured as the mean pixel intensity in the region of interest (ROI) (39.). The noise, in turn, is determined as the standard deviation (SD) of pixel intensity in the free air on an image (39). The recently developed parallel imaging technique, enhancing the speed of image acquisition has however an impact on calculating SNR. This technique is frequently used in FLASH 3D and volume interpolated breath hold (VIBE)

sequences, which were applied in our study. The major drawback of parallel imaging is a reduction of SNR due to decreased number of phase encoding steps. The loss of SNR in sequences using parallel imaging is approximately equal to the square root of the accelerating factor used (22). The so called 'g' factor is an additional downside of parallel imaging, which has an impact on SNR. The 'g' factor reflects an increase in local noise and is dependent on coil geometry, the orientation of phase-encoding direction, acceleration factor and the field of view as well as on the examined object (61). Its value may be calculated within pre-scan images (39). However, the GRAPPA (Generalized Autocalibrating Partially Parallel Acquisition (31)) algorithm affects the calculation of g factor and it may no longer be valid (67). The SNR measurements in parallel imaging techniques differ from regular calculation methods in conventional images due to a different estimation of noise. In conventional images, noise distribution follows the Gauss distribution and the noise is "spread" evenly across the image (54). In parallel imaging the noise distribution is inhomogeneous across the acquired image and follows the Rayleigh distribution (22). In some cases however obtaining the Gauss distribution is possible when the noise is estimated from the difference of the two images with high signal (67). Therefore two images have to be subtracted and the noise is determined as the SD of pixel intensity in the same ROI where the signal was measured in an unsubtracted image (18,62). The signal is proportional to the voxel size, the larger the voxel the higher the signal. The size of the voxel however is also depended on additional factors like field of view (FOV), number of phase encoding steps and slice thickness (ST) (36). In order to perform and compare the valid SNR measurements all above mentioned parameters must remain equal in sequences applied in different patients.

Contrast to noise ratio (CNR) has greater potential in determining the image quality than SNR (39,57). It is defined as the difference between the signal intensity of two different tissues (measured by ROI) to standard deviation of noise (39,57). In other words it is the

SNR difference between two different tissues divided by SD of noise. Both values (SNR and CNR) contribute to the objective image quality.

The exact equations applied in calculation of SNR and CNR are illustrated in the chapter (VI.1.6 Quantitative analysis).

III.4 Instrument Visualization in MR environment

The visualization of instruments differs in diverse imaging techniques. Excellent contrast between the instrument and surrounding tissue in X-ray can be obtained through the use of high-atomic number metals, which provide high attenuation of X-rays and render the instrument visible with high resolution. MR visualization of instruments is much more demanding and can be divided into passive and active (20). Interventional instruments can be detected inside the human body, which consists mainly of water molecules, by producing a signal void. This appears dark against the brighter tissue signal in the MR image. If the devices are made from metal or have metal components, they will cause an additional signal void due a susceptibility artifact. The susceptibility artifact is caused by local field inhomogeneity of the static magnetic field, which destroys the signal in this area. Local susceptibility artifacts can however be used to localize instruments (17). This is called passive visualization and makes the instrument directly visible as part of the standard MR image. Robustness, safety and simplicity are the main advantages of passive techniques. In the case of susceptibility markers material with high susceptibility (i.e., dysprosium oxide, iron oxide) is embedded into the instrument (i.e., catheter or guide wire) and produces a signal void. The drawback of this technique involves different marker sizes, which may be too large to depict them in detail in small vessels, or otherwise too small in larger vessels. In the case of positive markers, MR contrast agents based on gadolinium are effective since they can create a positive contrast when applied in the correct concentration (73). The general principle of this method consists of T1 time shortening by gadolinium derivatives. The minor drawback is that T1 weighted sequences have to be used to exploit this effect.

The active technique usually requires interaction between the instrument and the MR scanner. A microcoil, which is specially designed and tuned for this purpose, is fixed at the tip of the device and electronically connected to the scanner. The signal if the microcoil – and therefore the tip of the device – can be localized using projection data sets (20). The position of the device/microcoil can be projected on previously acquired image and the motion of the

instrument can be visualized (20). In cases of the patient's motion or sudden kinking of the vessel the simultaneous acquisition of microcoil position and the anatomic background is required (12). The main limitation of active tracking technique is the need for conductive wires, which may cause hazards for the patient due to the excessive heating of the tissues.

III.4.1 Guidewires

Guidewires (GWs) represent an essential tool for vascular interventions. Special type of guidewire (GW) was introduced in the beginning of the 80's by Terumo (Terumo, Tokyo, Japan) company. Its core is made of nitinol, a metal alloy mainly consisting of nickel and titanium. The term nitinol originates from these two metals and the place of origin (Naval Ordnance Laboratory, Maryland, USA) and is a finding of a Metallurgist William Buehler and Frederick Wang (1962) who were investigating a material that could be used in dismantling magnetic mines. Nitinol is non-ferromagnetic, superelastic and highly biocompatible and therefore it is widely used in production of hydrophilic GWs. Though not ferromagnetic, the metal core of nitinol GWs is conductive and therefore can act as an antenna during MRI. This may lead to substantial heating, which is a potential safety problem of nitinol GWs (56). Thus novel ideas concerning the manufacturing and construction of MR compatible wires were presented.

III.4.2 Catheters

Catheters can be used for various procedures in different anatomic regions with the help of various forms of tips and different fabrics employed during the manufacturing process. To achieve sufficient stiffness, many catheters have the so-called braiding, i.e., a metal mesh strengthens the body of the catheter. Most often, its made of stainless steel, which prompts the radiopacity. At the same time it makes those catheters unsuitable for the MR environment due to susceptibility artifacts and potential heating (30, 42, 56). Thus some catheters, especially the shorter ones, are built without any braiding. Those (pure plastic)

catheters are inherently safe in the MR environment. The non-braided catheters are however difficult to depict on an MR image due to their small size. For this reason and better passive navigation local metal markers can be placed along the shaft (2).

III.5 Safety aspects in MR environment

Static magnetic field strength of 9.4 T or less, which is currently applied in the diagnostic MR scanners, is considered not to pose any significant risk for humans. Nonetheless, the magnetic field can be dangerous especially when any metallic objects are brought close to the magnet field. Pacemakers or deep brain stimulator wires, as well as GWs and catheters used in endovascular procedures in interventional radiology, can be harmful to the human body due to their excessive heating and conductive properties (23, 35). Ferromagnetic implants can change their position in the human body while being placed in the magnetic field and thereby cause damage to surrounding organs. Electrical and non-electrical hospital equipment that regularly accompanies intensive care unit patients presents another safety issue since the magnetic field can cause their malfunctioning and they can be drawn in to the MR scanner.

III.5.1 Interventional instruments

As mentioned above, the hazards concerning placing metallic objects in the magnetic field are well known. According to Maxwell's theory, the temperature can arise from eddy currents induced by radiofrequency (RF) pulses and from induction loops build for example from electrocardiographic electrodes (23, 35, 42). In such cases there is no storage of electrical energy within the device (42). The energy however is cumulated when excessive heating is evoked around and within conductors (i.e., GWs or catheters) by resonating waves along them (42). If resonance of the GW occurs, the reflected waves are spreading along the longitudinal axis of the wire, which acts like a dipole antenna. In such scenario forming of standing RF waves is possible (42). The occurrence of resonance and hence the heating of a GW exposed to RF pulses depends on its position in a MR scanner, length, and if examined in a solution, on its immersed length (76). For example in the 1.5T MR scanner, the excessive heating hazard occurs when conductors longer then 15 - 18 cm are used (76). According to theoretical models, it can be assumed that the GWs shorter than a quarter of

the wavelength (i.e., 10.75 cm at 1.5 T) should be MR safe (76). The moment of occurrence of the resonance phenomenon is however troublesome to predict since it depends also on environmental factors (i.e., patient's weight, room temperature, etc.) and not only on the wire itself.

The paper of *Nitz et al.*(56) explains in detail the theory of coupling of wires with the MR field induced by a transmitter coils and heating effects at the ends of such a conductor. The authors performed several experiments with a standard nitinol GW (Terumo, Tokyo, Japan), that was placed in different positions (in and off center) of the MR scanner and suspended in the air as well as immersed in a saline solution filled phantom imitating the patient's tissue. The temperature alteration during real time gradient echo (GE) sequences was obtained by optical fiber temperature system (56). The results demonstrate that the voltage spreads towards both ends of a wire and the further the wire from the magnet isocenter the greater the temperature increase at the tip (56). The very relevant discovery is that the temperature increases also as a function of wire length and raised about 2°C in 170 cm and about 6°C in 156 cm wires. Since the temperature alterations were also observed at the tip of the wire inside the phantom (56), they could be potentially harmful to the patient. Hence, standard GWs cannot be used to perform endovascular MR guided interventions. Of note, in one of the studies sparks were observed at a distal tip of a standard GW as a mark of excessive heating (13).

III.5.2 Contrast media and intraarterial contrast agent application

Contrast media used in MR consist mainly of paramagnetic chelates of gadolinium (Gd) and are necessary in about 50% of MR examinations. The gadolinium-based contrast media increase the signal intensity on T1-weighted images by reduction of T1 relaxation time. Usually Gd-based contrast agents are applied intravenously and sometimes intraarticularly. The intraarterial (i.a.) application of MR contrast media, although performed in

several studies (29, 46) is performed off label. It is to assume that the kinetics after i.a.

administration are similar to i.a. application of iodinated contrast agents.

III.6 Role of interventional radiology in the therapy of hepatocellular carcinoma

Hepatocellular carcinoma (HCC) is the third most common cause of cancer death after lung and stomach cancer in poor developed countries and fifth after colorectal, breast and pancreas cancer in high developed countries (6). The incidence of HCC increases with advancing age in all populations in Europe (25). Most frequent risk factors, except from cirrhosis, include hepatitis C virus (HCV) (approximately 70% in Europe) and hepatitis B virus (HBV) (approximately 70% in east Asia and Africa). Among causes of cirrhosis and severe liver fibrosis the main factor encompasses increased alcohol uptake, non-alcoholic steatohepatitis (NASH) and inherited disorders like morbus Wilson, hemochromatosis or alfa-1-antitrypsin deficiency. It has been estimated that one third of individuals with liver cirrhosis will develop HCC during their lives (64). Additional risk factors include also nicotine abuse (71), diabetes (24) and obesity (51). The role of radiology is emphasized in the surveillance of cirrhotic and high-risk groups of patients, as well as in monitoring of disease stages with ultrasound, CT and MRI. In particular interventional radiology is highlighted in loco-regional treatment of moderate and advanced stages of HCC with radiofrequency ablation (RFA), transarterial chemoembolization (TACE), transarterial embolization (TAE) or selective internal radiation therapy (SIRT).

TACE is a recommended therapy method of choice in the intermediate stage of HCC without extrahepatic spread or vessel invasion (8, 9). Commonly it is also applied as a bridging therapy before liver transplantation or as a down-staging method before liver resection in HCC patients. Randomized controlled trials demonstrated that TACE achieves undeniable survival benefits in properly qualified patients as compared to best supportive care and it can prolong the survival up to 20 months (49) in the B stage according to Barcelona Clinic Liver Cancer (BCLC) criteria. The procedure itself is characterized by slow injection of chemotherapeutic agent (Doxorubicin, Cisplatin or/and Mitomycin C) and oily emulsion of iodinated contrast agent (Lipiodol), which has an embolic effect. This leads to tumor necrosis due to clotting of smaller tumor feeding vessels and results in delivery of the

chemotherapeutic agent directly to the HCC. Due to the tumor supply by hepatic artery vessels high doses of chemotherapy can be delivered to the tumor with relatively low systemic effects.

Camma et al. (15) found in their metaanalysis that segmental or subsegmental application of chemotherapy yields better treatment response in comparison to the embolization of the whole liver lobe. The HCC lesions due to its high arterial vessel supply is usually well recognizable in digital subtraction angiography (DSA). In some cases, if the tumor is atypically hypovascularised or after numerous previous TACE therapies, the lesion might not be visible under fluoroscopy. This may contribute to incorrect position of the catheter during application of chemotherapy and future poor therapy outcome. Catheters used to cannulate the celiac trunk have the diameters from 4F to 5F. Commonly used catheter shapes are cobra or sidewinder configurations. Selecitve and superselective cannulation of hepatic vessels is usually performed by smaller microcatheters (2.4F - 2.9F). In some cases larger catheters with hydrophilic coating suffice for this purpose.

IV STUDY OUTLINE

This study consists of two parts. The first part of the study focuses on determining the MR safe interventional instruments and on their validation in vascular models in a 1.5 T MR field. The devices characterized as MR safe and MR compatible are then applied in the second part of the study, which evaluates the liver tumor perfusion by i.a. transcatheter magnetic resonance angiography during transarterial chemoembolization in patients with hepatocellular carcinoma. The specific aims of each part are described below in section IV.1 and IV.2.

IV.1. SPECIFIC AIMS OF PART 1: MR safety of interventional instruments and their validation in vascular models

Transcatheter embolization is usually performed in an angiography suite only. The interventional instruments applied are mostly not MR safe due to their long metallic components, which may induce potentially harmful RF heating. The MR angiography part of the study requires however MR compatible and safe devices. Appropriate interventional instruments, like GWs or catheters especially designed for MR were not commercially available. Therefore we aimed to determine the potential use of novel prototypes of MR compatible GWs, which by that time were in the preclinical research phase. Before starting the clinical part of the study our aim was also to investigate the safety of instruments, regularly applied during TACE procedures in a 1.5 T MR scanner in a vessel model.

In this part of the study we aimed to answer the following question:

1. Does the novel prototype of MR compatible GW cause any increased heating in 1.5T MR filed as compared to a standard nitinol GW?

2. Is the novel prototype of MR compatible GW clearly visible on GRE MR images potentially applied during MR interventions?

3. Which catheters cause no artifacts on the MR image, due to lack of any

    metallic material incorporated and therefore are inherently MR safe?

IV.2. SPECIFIC AIMS OF PART 2: Evaluation of liver tumor perfusion by intraarterial transcatheter magnetic resonance angiography during transarterial chemoembolization in patients with hepatocellular carcinoma

The aim of this part of the study was to evaluate the liver tumor perfusion by i.a. transcatheter MR angiography during TACE in patients with HCC. The unexpected vascular supply or neoangiogenesis of the tumor may hamper TACE success and the unselective application of the chemoembolic agents may contribute to treatment-related liver failure (50,68). We aimed to investigate if MR angiography after transcatheter i.a. contrast agent application offers a possibility to identify the treated liver parenchyma. We hypothesized that this method can allow visualization of potentially new vascularisation or newly formed metastases or not perfused areas, that suggest tumor supply from another, extrahepatic collateral vessel. Hence, the interventional radiologist can change the primary therapy position of the catheter before final treatment, which may be significant for optimal tumor targeting.

In this part of the study we aimed to answer the following questions:

1. Is the performance of i.a. MR angiography during TACE feasible?
2. What is the optimal contrast agent concentration for i.a. MR angiography perfusion?
3. Which sequence is appropriate for i.a. perfusion studies: VIBE or FLASH 3D?
4. What are the benefits of i.a. transcatheter MR angiography during TACE?

V. PART 1: MR SAFETY OF INTERVENTIONAL INSTRUMENTS AND THEIR VALIDATION IN VASCULAR MODELS

V.1 Heating experiments with standard and MR compatible guidewires

V.1.1 Aorta model

V.1.1.1 Objectives

Several in vitro and animal trials using nitinol GWs have demonstrated excessive heating in the MR environment, rendering these devices unsafe for endovascular use (42, 56). A new MR compatible and MR safe GW has been developed recently (40, 41). We aimed to compare heating effects of this new MR compatible, polyetheretherketone (PEEK) GW with nitinol GW (Terumo, Japan) during different scenarios in MR imaging of a phantom.

V.1.1.2 Materials and Methods

The first 100 cm of the nitinol (Terumo, Tokyo, Japan) and MR compatible PEEK GW (Epflex, Dettingen, Germany) of the same length and diameter (145 cm, 0.89 mm) were immersed in a saline filled phantom (rubber tubes with 8 mm inner diameter, 2.4 mm wall thickness, **Figure 2**). The probes of a fiber-optic thermometer (Fotemp 4, OPTOcon AG, Dresden, Germany) were attached to the tip of the GWs with a thin thread. One of the probes (called reference probe) was also attached to the MR table as a reference probe for the temperature in the MR room. The accuracy of the measuring device was ± 0.2° Celsius (C). The aorta bifurcation of the phantom was exactly in the middle of a multichannel coil, which was wrapped around the phantom. The GW tip was placed 3 cm above the aorta bifurcation in all experiments. Balanced steady state free precession (bSSFP) (TE 1.6 milisecond (ms); time of repetition (TR) 3.5 ms; flip angle (FA) 60°; field of view (FOV) 40 cm; matrix 256 x 256) and spoiled gradient echo (SPGR) (time to echo (TE) 1.8 ms; TR 60 ms; FA 60°; FOV 40 cm; matrix 256 x 256) pulse sequences were acquired in a 1.5 T MR scanner with use of an 8-channel array coil (GE Medical Systems, Waukesha, WI, USA). Temperatures were

recorded with 1 second (s) temporal resolution while the phantom was placed centrally in the bore of MR scanner and in an off-center position (x = 24 cm, y = -5 cm, z = -10/10 cm). The bSSFP sequence was run for 1 minute and the SPGR sequence for 12 minutes. The estimated specific absorption rate (SAR) for every sequence equaled 1.15 W/kg. The peak SAR for every sequence equaled 2.30 W/kg.

Guidewires

MR compatible guidewire

A novel PEEK GW (Epflex, Dettingen, Germany) of 0.89 mm diameter and 145 cm length was examined. The GW consists of PEEK and Pebax tip with 3 iron-oxide markers ("MagnaFy", Nano4imaging, Aachen, Germany) integrated into the tip and 3 markers behind the tip. The markers allow passive visualization due to the creation of susceptibility artifacts.

Nitinol-based guidewire

A nitinol GW (Terumo, Tokyo, Japan) was used as comparison. The GW has a nitinol alloy core. The core is moreover covered with tungsten in a polyurethane jacket to create radiopacity under X-ray fluoroscopy. A hydrophilic coating provides gliding properties. The same diameter and length as in the MR compatible GW were selected (0.89 mm diameter, 145 cm length).
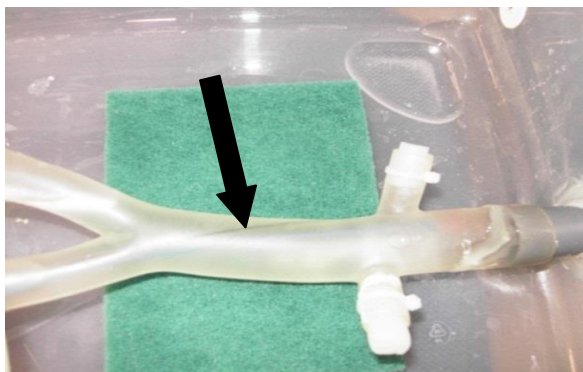
Figure 2
Aorta shaped phantom with nitinol-based
GW, black arrow is pointing a GW.

V.1.1.3 Results

bSSFP sequence acquisition for 60 seconds

In the first scenario, when the nitinol GW was placed in the isocenter of a 1.5T MR scanner during a 60 seconds bSSFP sequence, only minor temperature changes of both GWs were observed. The temperature of the nitinol GW increased from initially 20.3°C to a maximum of 20.6 °C (**Figure 3**). Temperature changes within the measurement error of the fiber-optic thermometer (± 0.2°C) of 0.1°C were observed for the PEEK GW. The reference probe attached to the MR scanner table did not change the temperature (20.3 °C).

The second position in the MR scanner, when the aorta phantom was placed eccentrically close to the MR scanner walls, was performed to simulate the worst case scenario for possible heating. The temperature of a nitinol GW in this off-center position rose from initial 20.3°C to 29.9°C (**Figure 4)**. The PEEK GW demonstrated no relevant temperature elevation. The reference probe demonstrated a minimal increase of temperature of 0.1°, which was within the measurement error interval of the fiber-optic thermometer (± 0.2°C).

SPGR acquisition for 720 seconds

The second sequence, i. e. the SPGR, was run continuously for 720 seconds (i. e. 12 minutes) in order to imitate the duration of imaging during the endovascular intervention. Results of these experiments are presented in **Figure 5** and **Figure 6**. As demonstrated in **Figure 5**, during 720 seconds the temperature at the nitinol GW tip increased from 20.3°C to 21.4°C when the phantom was placed centrally in the magnet bore. The PEEK GW demonstrated a maximum temperature elevation of 0.4°. The reference probe showed a temperature increase from 20.4°C up to 20.8°C. Both temperature changes of PEEK GW and the reference probe were within the measurement error of the fiber-optic thermometer (± 0.2°C).

The off-center position demonstrated the temperature increase for the nitinol GW from 21.8°C to 34.8°C (**Figure 6**). The same experiment repeated with the MR compatible PEEK GW demonstrated a temperature elevation of 0.1°. The reference probe showed an increase from 21.2°C to 21.3°C.
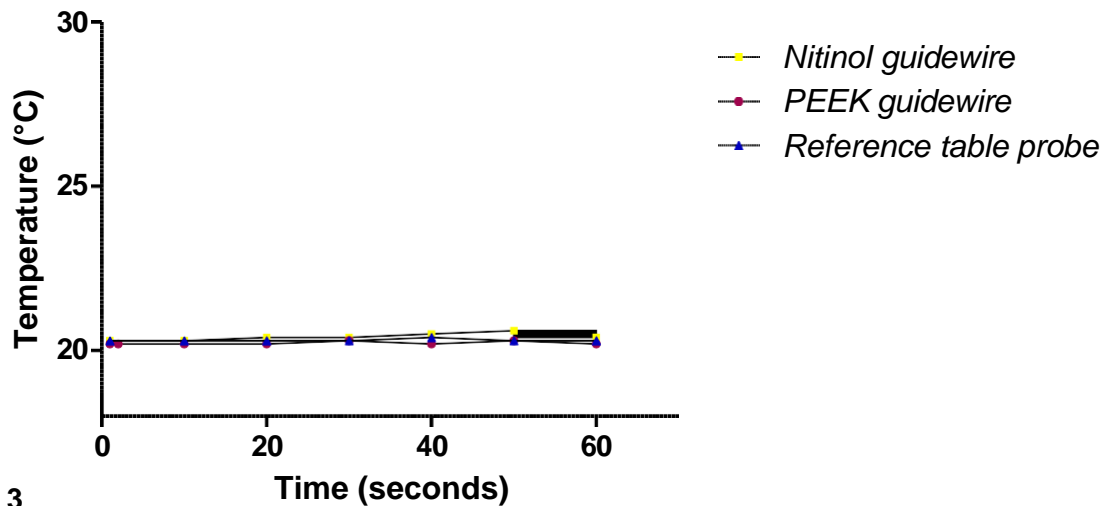
Figure 3
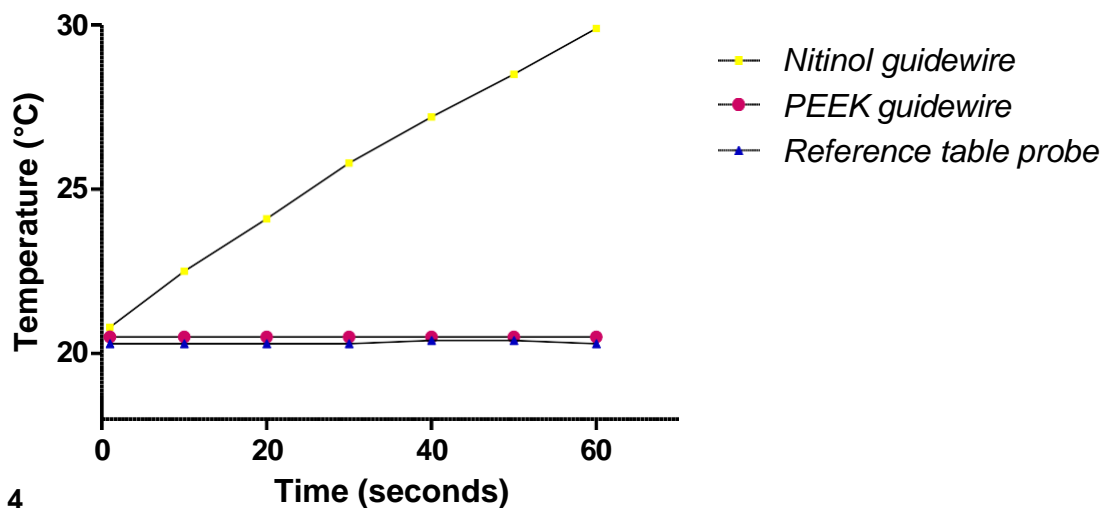Nitinol GW (yellow) and MR compatible PEEK GW (red) imaged with bSSFP sequence for 60 seconds in in center position.

Figure 4
Nitinol GW (yellow) and MR compatible PEEK GW (red) in bSSFP sequence for 60 seconds in off center position.
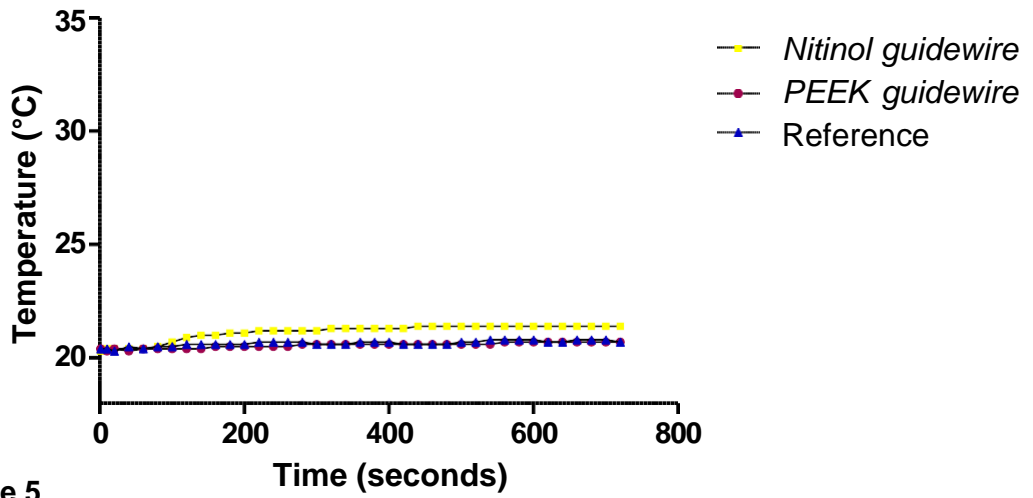
Figure 5
Minor temperature fluctuation of nitinol GW (yellow) comparing to PEEK GW (red) during SPGR imaging for 12 min in in center position in the scanner.
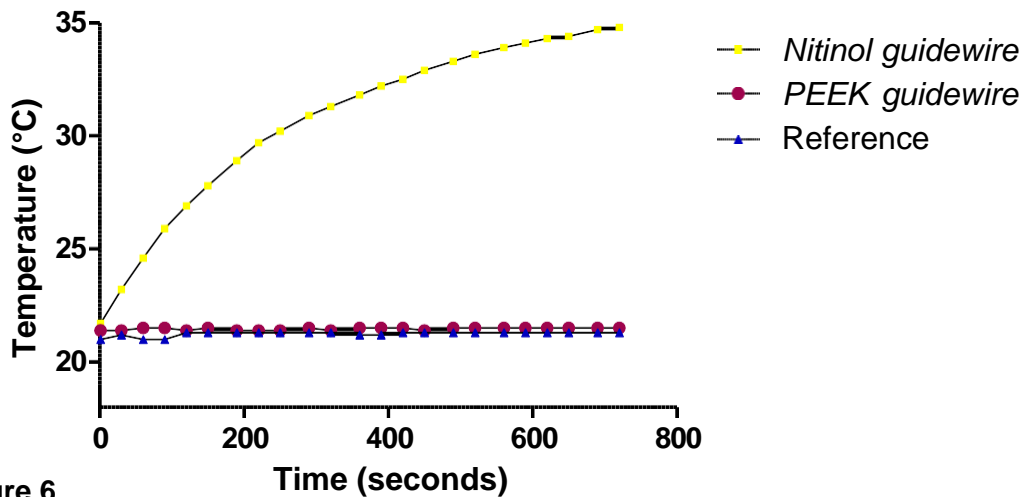
Figure 6
The 13° temperature elevation of nitinol GW (yellow) comparing to minor temperature variations of the PEEK GW (red) during SPGR imaging for 12 min in off center position in the scanner.

V.1.1.4 Conclusions

The temperature of the nitinol GW increased by 0.3°C (center) and 1.1°C (off-center position) while use of the bSSFP and by 9.6°C and 13°C (off-center position) while use of the SPGR sequence. Only minor temperature changes up to a maximum of 0.4°C were observed with the MR compatible PEEK GW in any applied position or sequence. The prototype of a MR compatible PEEK GW shows substantially lower heating than a standard nitinol GW in bSSFP or SPGR imaging sequences in a phantom. The novel PEEK GW demonstrated a potential for endovascular MR interventions due to the lack of heating during the procedure.

V.1.2 Thiel embalmed human cadaver and vascular phantom

V.1.2.1 Objectives

The aim of this study was to measure a heating temperature while retracting a nitinol based GW in a saline filled phantom and in the vessels of a Thiel embalmed human cadaver to find the maximal RF-heating due to resonance effect. The near-real time MR imaging as continuously run SPGR sequence was applied in 1.5 T MR Scanner (Signa HDxt, GE Healthcare Systems, USA). The local ethics committee approval was obtained before starting the experiments. To check the cooling effect of a blood flow we simulated similar conditions in the femoral artery of a human cadaver with saline solution.

V.1.2.2 Materials and Methods

A 0.89 mm nitinol-based GW with a length of 145 cm (Terumo, Tokyo, Japan) was immersed over the length of 85 cm in a 260 ml saline filled phantom. The probes of fiber-optic thermometer (Fotemp 4, OPTOcon AG, Dresden, Germany) were attached to the tip, 20 cm from the proximal end and to the distal end of the GW. One reference probe was attached to the MR table. Initial temperature of all probes was 20.9°C. The accuracy of the measuring device was ±0.2°C. The temperature changes of a nitinol GW were recorded while running a SPGR sequence (TR 60 ms; TE 1.8 ms; FA 60°; FOV 40 cm; matrix 256 x 256) for 5 minutes. Then the nitinol GW was retracted 2 cm every 10 seconds while running the same sequence for another 5 minutes. Only one temperature probe was attached to the tip of the GW in the human cadaver experiment. The Terumo GW was placed under X-ray guidance in the left common iliac artery with initial tip temperature of 21.5°C. The GW was retracted with the same speed as previously while running the same sequence and temperature was recorded. Afterwards the GW was placed again in the left femoral artery and the measurements were taken after inducing a saline flow of 1.6 ml/s. All temperature curves were recorded with 1s temporal resolution. Experimental setups are summarized in **Table 1**.

Phantom	Cadaver
Saline filled (260 ml)	Artificially induced saline flow 1.6 ml/s, GW in the left iliac artery
Initial temperature 20.9°C	Initial temperature 20.9°C
Fiber-optic thermometer probes: - GW tip - 20 cm from proximal end - end of a GW	Fiber-optic thermometer probes: - GW tip
FLASH sequence for 5 min	FLASH sequence for 5 min
Retracting a GW every 10 sec	Retracting a GW every 10 sec

Table 1
Experimental setup of a GW heating analysis in a phantom and cadaver.

V.1.2.3 Results

The results are summarized in **Table 2**. The maximum temperature increase of the nitinol GW observed in the phantom study without retraction of the GW was from 20.9°C to 24.9°C measured at the GW tip. The highest temperature of 25.4°C was observed in the probe attached 20 cm from the proximal GW end in the phantom experiment with retraction. The temperature of a Terumo GW did not show a relevant change in the iliac vessel (maximum 22.8°C without flow or retracting and 23.1°C with flow retracting respectively). The cooling effect of saline flow showed no relevant influence on the temperature changes of the nitinol GW which increased by 2.2° with and by 2° without retracting a GW.

Experiment number	Experimental setup in different scenarios		
Experiment 1	**Aorta phantom without retraction**		
	Max. temperature at:		
	tip of a GW	20 cm from the prox. End of a GW	End of a GW
	24.90°C	21.60°C	24.70°C
Experiment 2	**Aorta phantom with retraction**		
	Max. temperature at:		
	tip of a GW	20 cm from the prox. End of a GW	End of a GW
	24.40°C	25.40°C	21.20°C
Experiment 3	**Thiel-embalmed human cadaver without flow or retraction**		
	Max. temperature at:		
	tip of a GW	-	-
	22.80°C	-	-
Experiment 4	**Thiel-embalmed human cadaver with saline flow and without retraction**		
	Max. temperature at:		
	tip of a GW	-	-
	23.00°C	-	-
Experiment 5	**Thiel-embalmed human cadaver with saline flow and with retraction**		
	Max. temperature at:		
	tip of a GW	-	-
	23.00°C	-	-

Table 2 Nitinol-based GW in different scenarios in 1.5T MR scanner.

V.1.2.4 Conclusions

Retraction of the GW in a vessel model and in Thiel-embalmed human cadaver did not have any significant influence on the measured temperature in our experiments. Nonetheless, it is not possible to conclude that all GWs are MR safe. Conditions creating resonance and consequently substantial heating might still occur for electrically conducting wires and instruments (26). Artificially induced saline flow in a vessel of a human cadaver did not show any substantial cooling effect on nitinol GW independent on retraction procedure, but this might be due to the relatively low increase in temperature during our experiments even without flow.

V.2 Artifact size of a new MR compatible guidewire prototype depends on time to echo in gradient echo sequences

V.2. 1 Objectives

As mentioned before, lack of appropriate devices hinders the endovascular interventions under MR guidance. GWs composed of nickel and titanium alloys or stainless steel were proven to be unsafe and not fully MR compatible due to RF heating, which is caused by their conductive properties. Glass fibers embedded in epoxy resin are considered to be a metal free alternative in a novel GW (MaRVis, Aachen, Germany). To enable the passive visualization under MR guidance special iron-oxide markers are immersed at the tip and along the GW core. GE sequences generally cause greater artifacts as compared to spin echo (SE) sequences. However, MR guidance of vascular interventions is usually performed by GE sequences. Aim of this study was to test the passive visualization of the novel MR compatible GW (MaRVis, Aachen, Germany) by GE FLASH 3D sequence using different TE times in 1.5 T MR scanner (Aera, Siemens Medical, Erlangen, Germany).

V.2.2 Materials and Methods

A flexible type of a novel MR compatible GW (MaRVis, Aachen, Germany), with the diameter of 0.89 mm and length of 145 cm was tested in a glass made, aorta shaped phantom. The phantom was made of thin glass and was immersed in a water bath with diluted MR contrast agent (1.0% Gadolinium-gadobenate dimeglumin (Gd-BOPTA), Multihance® (Bracco, Milan, Italy)). The GW were immersed by approximately 1/2 of its length (**Figure 7**). The GW was imaged with straight configuration in the main lumen of the aorta and curved into the right renal artery. Different TE from 1.07 to 20 ms was employed during the FLASH 3D GE sequence (TR 4.89 - 21.85 ms [shortest TR depending on TE], FOV 400 mm, matrix 512 x 101, ST 0.8 mm, FA 25°, number of slices 5). Obtained images were evaluated according to the artifact size of the GW.

Inserted GW
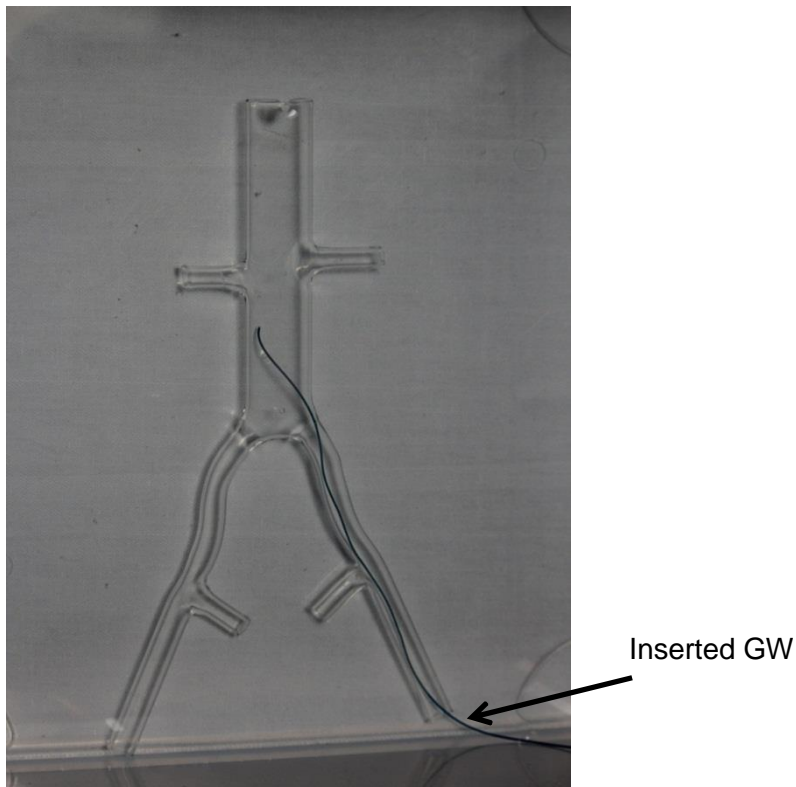
Figure 7
Aorta shaped model in a saline bath.

V.2.3 Results

The artifact size depends strongly on applied time to echo (TE) and increases with the echo time. The best passive visualization (defined as smallest GW artifact) was achieved with the minimal TE of 1.07 ms for both GWs. TE greater than 10 ms hinders the recognition of the GW core due to interference of the markers in both GW types and obstructs the visibility of the 5 mm diameter renal artery of the aorta phantom. There were no differences in visualization between the stiff and flexible GWs. The images of GW are presented in the **Figures 8-9**. Please note that depending on TE time TR varies from 4.89 ms with TE 1.07 ms to TR 21.85 ms with TE 20 ms.
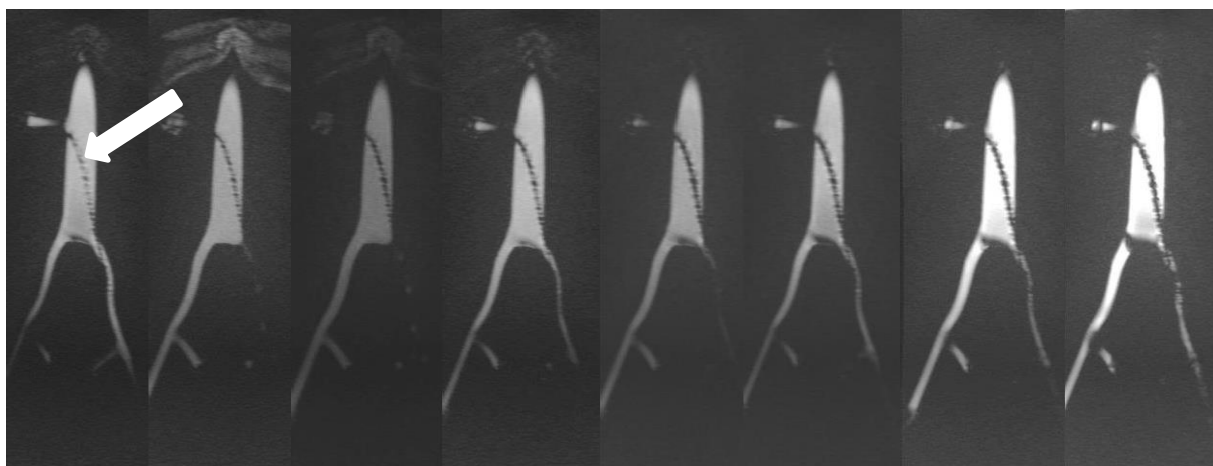
TE 1.07   TE2 ms   TE3 ms   TE4 ms   TE5 ms   TE6 ms   TE10 ms   TE20 ms

Figure 8
MaRVis flexible GW 0.89 mm, 145 cm straight depicetd in the aorta phantom with the tip
of the GW directly below the right renal artery. White arrow points to a GW.
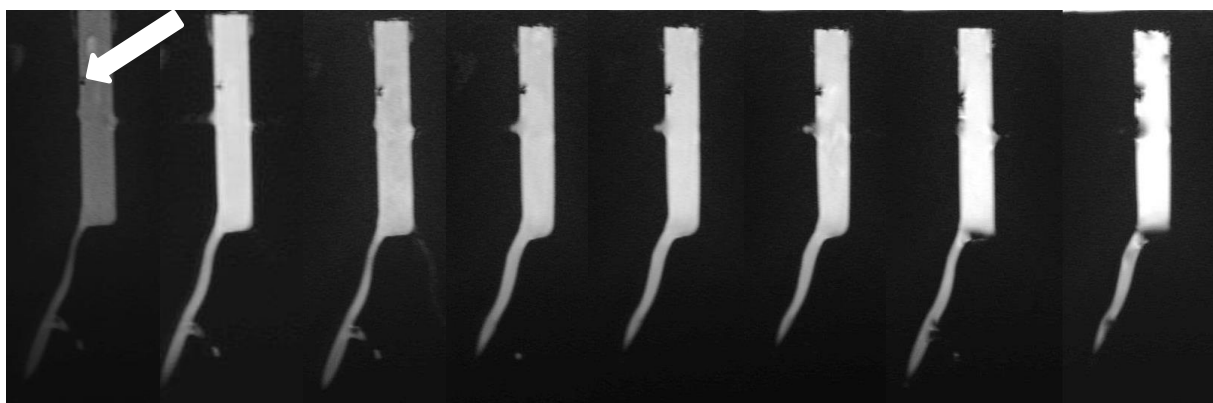
TE 1.07   TE2 ms   TE3 ms   TE4 ms   TE5ms   TE6ms   TE10 ms   TE20ms

Figure 9
MaRVis flexible GW 0.89 mm, 145 cm straight positioned in the aorta phantom with the tip
of the GW above the right renal artery. White arrow points to a GW.

V.2.4 Conclusions

The markers used in the GW make passive visualization possible applying a FLASH

3D GE sequence. As expected, the lowest achievable TE was the best for depicting both

GWs. The novel MR compatible GW is excellent depicted with low TE in GE sequences.

V.3 Passive visualization of catheters in a vascular model

V.3.1 Objectives

Catheters and GWs are essential equipment in every angiography suite. Different types of catheters have different braiding (i.e., a metal mesh), which provides the desired rigidity, pushability and make them visible under fluoroscopy. This braiding prevents artifact-free visibility under MR guidance and causes potential harm to the patient due to RF heating. Aim of this study was to evaluate the visibility and test the MR compatibility of 13 different angiographic catheters in vitro in two vessel models.

V.3.2 Materials and Methods

Thirteen regular catheters from Cook Medical (Bloomington, USA), Terumo (Tokyo, Japan) and Optimed Alta Flow Measuring catheters (Ettlingen, Germany) company with length of 65 and 100 cm, external diameter of 4F and 5F and differently shaped tip (cobra, straight, shepherd hook, pigtail, sidewinder) as well as 3 different microcatheters (Terumo, Tokyo, Japan and Cook Medical, Bloomington, USA) with diameters of 2.4F, 2.7F and 2.8F were tested. All catheters were first tested in a vessel model (Elastrat, Geneva, Switzerland, **Figure 10**) filled with 0.9% saline solution mixed with 1.0% of Gd-BOPTA, Multihance® (Bracco, Milan, Italy). The financial support for the model was assured by IIIOS Project (The Integrated Interventional Imaging Operating System (IIIOS) project funded by the European Community's Seventh Framework Programme (FP7/2007 -2013) under Grant Agreement no 238802). The first model consists of two parts, the femoral and the tibial one and a 3 liter fluid tank connected to the phantom. The specially designed introducer (**Figure 11**) allows insertion of a sheath through a silicon pad. The GWs and catheters are inserted through commercially introducer sheaths of 5F (Radifocus, Terumo, Tokyo, Japan). The diameters of each vessel respond the normal anatomic diameters of the vessels. The flow within the model is generated by a pump, which is located within the water tank. Then the catheters

were tested in glass-made, aorta-shaped model used in previous experiment (chapter V.2, Figure 7). Three T1 weighted GE sequences and one T2 weighted FSE sequence were applied (sequence1 GE FLASH two-dimensional (2D): TR 127 ms, TE 5.36 ms, FA 70°, ST 8 mm, matrix 736 x 467; sequence2 GE FLASH 3D: TR 3.41 ms, TE 1.3 ms, FA 25°, ST 2 mm, matrix 512 x 448; sequence3 VIBE: TR 3.73 ms, TE 1.21 ms, FA 12°, ST 4 mm, matrix 320 x 147; sequence 4 TSE T2 weighted: TR 3.690 ms, TE 85 ms, FA 180°, ST 10 mm, matrix 768 x 468). All experiments were performed on a 1.5 T MR scanner (Aera, Siemens Medical, Erlangen, Germany) using the body array coil.
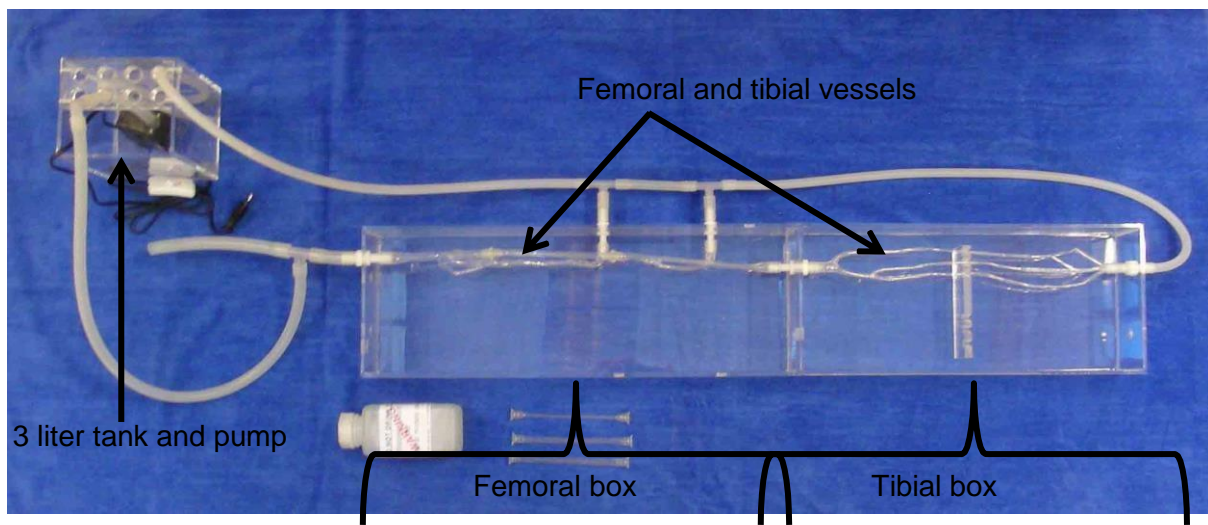
Figure 10
Vessel model of the left lower extremity (Elastrat, Geneva, Switzerland).

Figure 11
Introducer in the vessel model of the left lower extremity (Elastrat, Geneva, Switzerland).

V.3.3 Results

All images are summarized in **Tables 3-11**. Catheters with hydrophilic coating from Terumo company (5F and 4F Cobra of 65 and 100 cm length as well as 5F Sidewinder of 100 cm length), demonstrated no significant artifacts and good visualization of the shaft and tip without blurring effect, in particular in the aorta shaped glass phantom (**Tables 3-6**) and also in the Elastrat vessel model (**Table 7**). The TSE T2 weighted sequence was the most sensitive in depicting the catheters. The 4F catheters (Alta Flow Measuring catheters family: straight and pigtail like, Optimed, Ettlingen, Germany) demonstrated also no susceptibility artifacts (**Tables 8** and **9**). The Progreat microcatheters 2.4F, 2.7F and 2.8F (Terumo, Tokyo, Japan) demonstrated no susceptibility artifacts during imaging in either of the applied sequences, the 2.8F Cantata microcatheter (Cook Medical, Bloomington, USA) showed however a substantial susceptibility artifact along the entire shaft, making the catheter not recognizable (**Table 10**). The latter five commercially available catheters (Cook Medical, Bloomington, USA) with differently shaped tips (5F cobra 100 cm, 4F straight 65 cm, 4F pigtail 65 cm, 5F sidewinder 100 cm, 5F shepard hook 65 cm) demonstrated major susceptibility artifacts probably due to their double braiding with metal mesh from stainless steel (**Table 11**). Among latter catheters the 4F Pigtail 65 cm and 5F Sidewinder 100 cm showed substantially less artifacts at 15 cm distal section, the rest of the shaft demonstrated artifacts even larger than the iliac vessels of the aorta model.
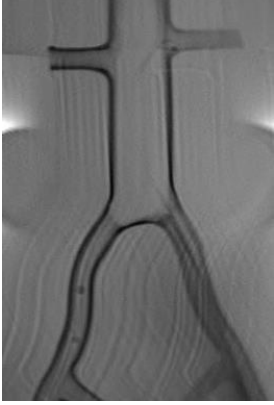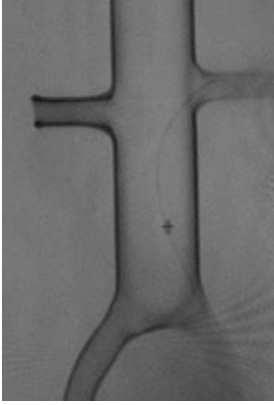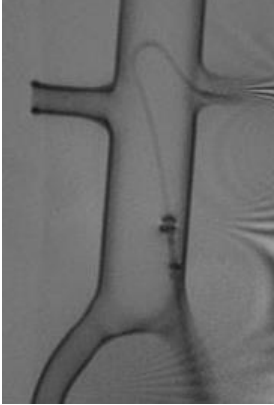
Catheter type	Sequence type: FLASH 2D
4F Cobra 65 and 100 cm	
5F Cobra 65 and 100 cm	
5F Sidewinder 100 cm	

Table 3
Cobra 4F, 5F and 5F sidewinder (Terumo, Tokyo, Japan) in aorta shaped model filled with saline and 1% Gd-BOPTA (Multihance, Bracco, Milan, Italy) solution. FLASH 2D sequence.
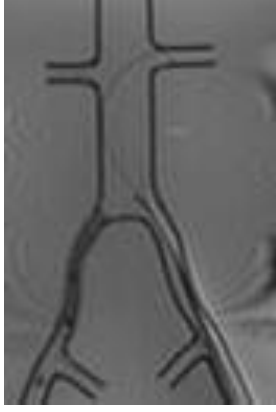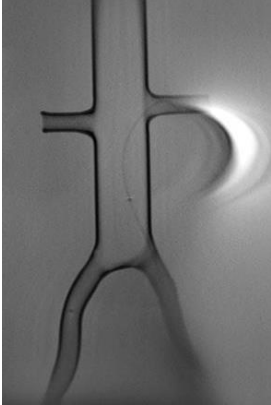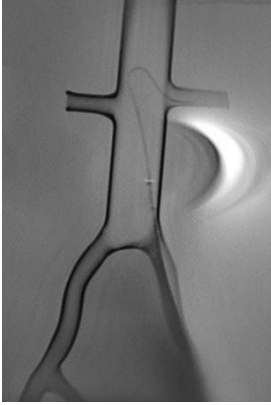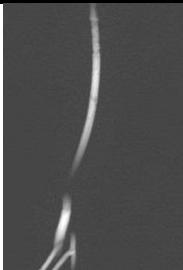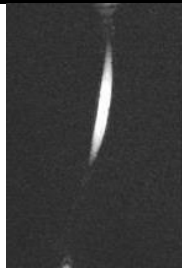
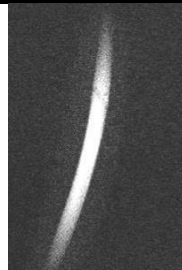| Catheter type	Sequence type: FLASH 3D
4F Cobra 65 and 100 cm	
5F Cobra 65 and 100 cm	
5F Sidewinder 100 cm	

Table 4
Cobra 4F, 5F and 5F sidewinder (Terumo, Tokyo, Japan) in aorta shaped model filled with saline and 1% Gd-BOPTA (Multihance, Bracco, Milan, Italy) solution. FLASH 3D sequence.

Catheter type	Sequence type: VIBE
4F Cobra 65 and 100 cm	
5F Cobra 65 and 100 cm	
5F Sidewinder 100 cm	

Table 5
Cobra 4F, 5F and 5F sidewinder (Terumo, Tokyo, Japan) in aorta shaped model filled with saline and 1% Gd-BOPTA (Multihance, Bracco, Milan, Italy) solution. VIBE sequence.

Catheter type	Sequence type: TSE T2 weighted
4F Cobra 65 and 100 cm	
5F Cobra 65 and 100 cm	
5F Sidewinder 100 cm	

Table 6
Cobra 4F, 5F and 5F sidewinder (Terumo, Tokyo, Japan) in aorta shaped model filled with saline and 1% Gd-BOPTA (Multihance, Bracco, Milan, Italy) solution. TSE T2 weighted sequence.
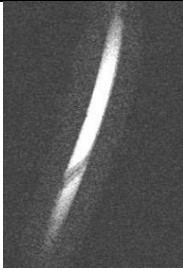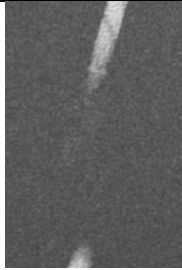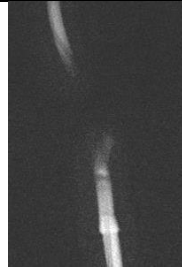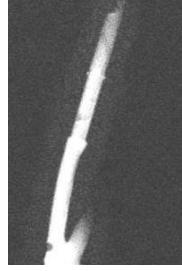
Catheter type	Sequence type			
	FLASH 2D	FLASH 3D	VIBE	TSE T2 weighted
4F Cobra 65 and 100 cm				
5F Cobra 65 and 100 cm				
5F Sidewinder 100 cm				

Table 7
Cobra 4F, 5F and 5F sidewinder (Terumo, Tokyo, Japan) in vessel phantom, placed in the left superficial artery (Elastrat, Geneva, Switzerland) filled with saline and 1% Gd-BOPTA (Multihance, Bracco, Milan, Italy) solution. FLASH 2D, FLASH 3D, VIBE and TSE T2 weighted sequence.
Note: Only crucial parts of catheters are depicted in the curved course of the vessel.
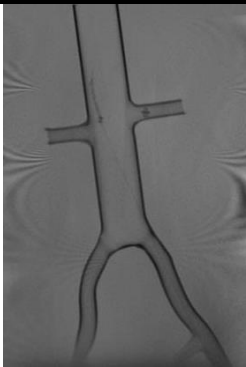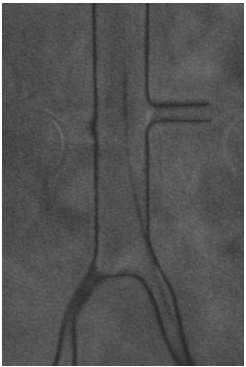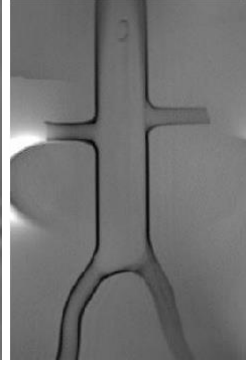
Catheter type	Sequence type			
	FLASH 2D	FLASH 3D	VIBE	TSE T2 weighted
4F straight Alta Flow Premium catheter (Optimed, Germany)				
4F pigtail like Alta Flow Premium catheter (Optimed, Germany)				

Table 8
4F straight and pigtail shaped Alta Flow Premium catheter (Optimed, Germany) in the aorta shaped phantom filled with saline and 1% Gd-BOPTA (Multihance, Bracco, Milan, Italy) solution. FLASH 2D, FLASH 3D, VIBE and TSE T2 weighted sequence.

Catheter type	Sequence type			
	FLASH 2D	FLASH 3D	VIBE	TSE T2 weighted
4F straight Alta Flow Premium catheter (Optimed, Germany)				
4F pigtail like Alta Flow Premium catheter (Optimed, Germany)				

Table 9
4F straight and pigtail like Alta Flow Premium catheters (Optimed, Germany) in the vessel phantom (Elastrat, Geneva, Switzerland) filled with saline and 1% Gd-BOPTA (Multihance, Bracco, Milan, Italy) solution. FLASH 2D, FLASH 3D, VIBE and TSE T2 weighted sequence.
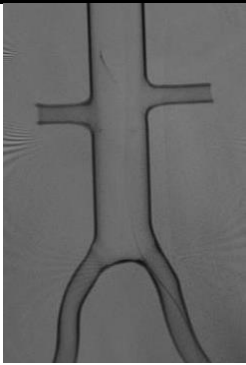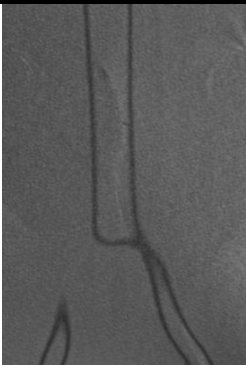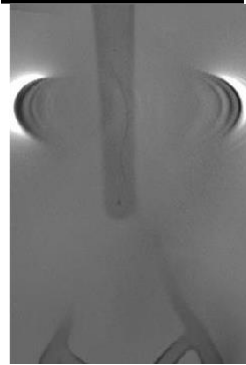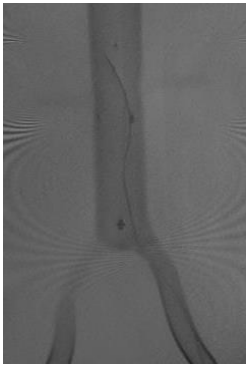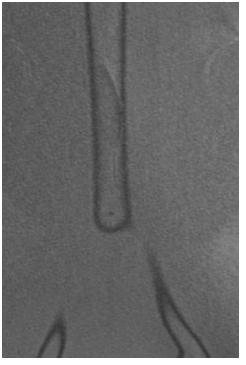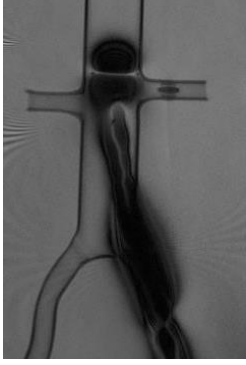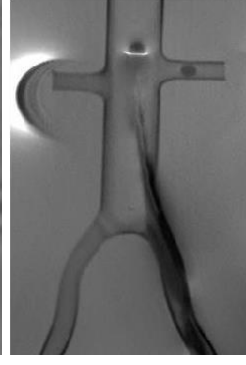
Catheter type	Sequence type			
	FLASH 2D	**FLASH 3D**	**VIBE**	**TSE T2 weighted**
Progreat microcatheter 2.4F (Terumo, Japan)				
Progreat microcatheter 2.7F (Terumo, Japan)				
Cantata microcatheter 2.8F (Cook Medical, USA)				

Table 10
Progreat microcatheter 2.4 and 2.7F (Terumo, Japan) and Cantata microcatheter 2.8F (Cook Medical, USA) in a aorta shaped phantom filled with saline and 1% Gd-BOPTA (Multihance, Bracco, Milan, Italy) solution. FLASH 2D, FLASH 3D, VIBE and TSE T2 weighted sequence.
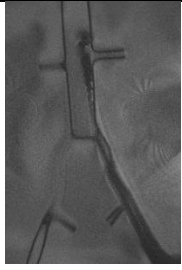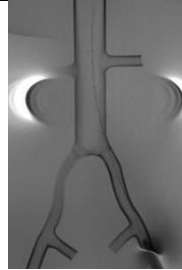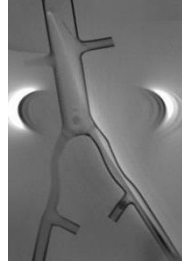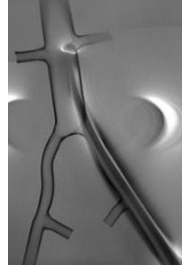
Catheter type	Sequence type			
	FLASH 2D	FLASH 3D	VIBE	TSE T2 weighted
5F Cobra 100 cm (Cook Medical)				
4F Straight 65 cm (Cook Medical)				
4F Pigtail 65 cm (Cook Medical)				
5F Sidewinder 100 cm (Cook Medical)				
5F Shepard Hook 65 cm (Cook Medical)				

Table 11
5F cobra 100 cm, 4F straight 65 cm, 4F pigtail 65 cm, 5F sidewinder 100 cm, 5F shepherd Hook 65 cm (Cook Medical, USA) in a aorta shaped phantom filled with saline and 1% Gd-BOPTA (Multihance, Bracco, Milan, Italy) solution. FLASH 2D, FLASH 3D, VIBE and TSE T2 weighted sequence.
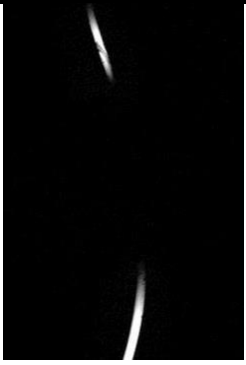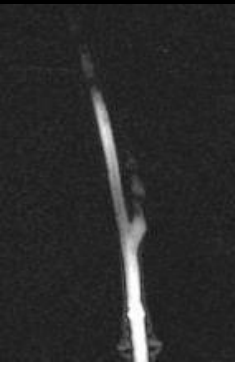
V.3.4 Conclusions

The catheters with hydrophilic coating (Cobra, Terumo) show no susceptibility artifact in any of the four tested sequences. The Optimed company offers a promising solution with excellent visibility of non-braided straight and pigtail shaped catheters. Microcatheters (Terumo) with 2.4F and 2.7 F diameters showed also MR compatibility with good image depiction. The lack of susceptibility artifacts proves that no metallic parts are being integrated into the catheters. Therefore, these catheters are considered MR safe. Other regular catheters are excluded from the second part of the study since they may pose a potential risk to the tissue due to potential RF heating. In addition, their image artifacts make them unsuitable for MR guided interventions.

VI. PART 2: EVALUATION OF LIVER TUMOR PERFUSION BY INTRAARTERIAL TRANSCATHETER MAGNETIC RESONANCE ANGIOGRAPHY DURING TRANSARTERIAL CHEMOEMBOLIZATION IN PATIENTS WITH HEPATOCELLULAR CARCINOMA

VI.1 Materials and Methods

VI.1.1 Study design

This prospective study was performed in the Clinic of Diagnostic and Interventional Radiology at Saarland Medical Center in Homburg in Germany from the 29.02.2012 to 04.12.2012. The angiographies were performed on an Artis live and Artis zee angiography devices (Siemens Medical, Erlangen, Germany). The magnetic resonance imaging was performed on 1.5 T Aera MR Scanner with 70 cm diameter wide bore (Siemens Medical, Germany). All patients participating in the study signed the informed consent at least one night prior to the procedure. The local ethics committee approved this prospective study.

VI.1.2 Patients

The cohort consisted of 27 patients (21 men, median age 61 years old). A total of 62 TACE procedures with i.a. contrast agent application in MR were performed. The cohort was divided into two subgroups. The first subgroup encompassed 9 patients, in this subgroup overall 13 TACE procedures were performed. In these patients different contrast agent concentrations (from 0.5% to 10.0%) were applied during MR examination. The results of this qualitative analysis allowed us to determine the appropriate contrast agent concentration for the procedures in the second, larger subgroup. Detailed description of analysis is provided in the chapter VI.1.5. The second subgroup consisted of 18 patients in whom 49 TACE procedures were performed. Here, the selected contrast agent concentration was injected and two GE sequences were applied. Detailed description of quantitative analysis is provided in the chapter VI.1.6.

Overall, a single TACE procedure was performed in 10 patients, in the remaining 17 patients multiple TACE procedures were conducted. The detailed characteristics of the patients are summarized in **Table 12**. All patients were qualified for TACE either as palliative or bridging approach before liver transplantation during a multidisciplinary conference. Inclusion criteria were in line with the latest European guidelines and were as follows (*EASL: European Association For The Study Of The Liver; EORTC: Organisation For Research And Treatment Of Cancer clinical practice guidelines: management of hepatocellular carcinoma* (21)): age more than 18 years old, Child Pugh class A or B, focal or multifocal HCC, no contraindication against MR imaging (i.e., pacemaker, metal implants, claustrophobia), signed informed consent. Exclusion criteria were uncorrectable coagulopathy (Quick < 50%) or thrombocytopenia (< 50 000/ ul), serum creatinin level >2 mg/Dl, complete portal vein thrombosis of the main trunk, Child Pugh class C, life expectancy less than 6 months and lack of informed consent. Patients with thrombosis of only one branch of the portal vein were enrolled in the study. One patient with cholangiocellular carcinoma (CCC) was enrolled in the study but due to the progression of the disease after TACE was qualified for systemic chemotherapy. One patient with liver metastases of colon carcinoma and one with metastases of urothelial carcinoma of the bladder were also included in the study after revising the indications during the weekly tumor board conference. The diagnosis of HCC was mostly performed by contrast enhanced CT, sonography or MR scan according to well-established perfusion patterns. A total of 5 patients underwent a biopsy to confirm the diagnosis. Detailed clinical characteristics are provided in **Table 13**.

Patients characteristics	
Number of patients	27
Number of TACE procedures	62
Age (median)	61 years old
(range)	35-86 years old
Gender:	6 females
	21 males
Prior treatment	8 TACE
	4 Resection
	2 RFA
	1 SIRT
Diagnosis of HCC	21 MR
	5 Biopsy
	1 CT

Table 12 Patients characteristics.
Abbreviations:
TACE, transarterial chemotherapy; RFA, radiofrequency ablation; SIRT, selective internal radiation therapy; MR, magnetic resonance; CT, computed tomography

Clinical characteristics	Number of patients
Tumor type	
• *HCC*	24
• *CCC*	1
• *Metastases*	2
Right liver lobe	17
Left liver lobe	4
Bilobar	6
Portal vein branch thrombosis	3
Cirrhosis	24
Cause of liver cirrhosis	
• *Alcohol*	8
• *Hepatitis C virus*	7
• *Hepatitis B virus*	4
• *Unknown*	2
• *Alfa 1 antritripsin deficiency*	1
• *Haemochromatosis*	1
• *Autoimmune hepatitis*	1
Child- Pugh score in patients with liver cirrhosis (N = 24)	
• *A*	17
• *B*	7

Table 13 Summary of clinical characteristics

VI.1.3 Procedure details and workflow

Procedure details

Every procedure began with local anesthesia (2% Mepivacain) applied after shaving the right groin and draping the patient in sterile fashion. Then the right common femoral artery was punctured with 18G needle (Terumo, Tokyo, Japan) and a 5F or 6F sheath (Radifocus, Japan) was inserted over a 0.89 mm hydrophilic GW (Terumo, Tokyo, Japan) using the modified Seldinger technique. The celiac trunk and hepatic artery were cannulated using the previously tested 4F/5F cobra or sidewinder shaped catheters with hydrophilic coating (Terumo, Tokyo, Japan). The smaller caliber branches of hepatic arteries were cannulated using the 2.4F -2.9F microcatheters (Progreat, Terumo, Tokyo, Japan). DSA was performed either manually or automatically (2 ml/s) with iodinated contrast agent (Imeron 300, Bayer Schering Pharma, Berlin, Germany) to confirm the correct therapy position of the catheter. In cases when the therapy position was difficult to estimate, for example due to multiple tumors or lack of tumor visualization, the catheter was left in the main trunk of right or left hepatic artery. After removing all metal and non-MR compatible objects from the angiography table, the patients were transferred into the MR unit in order to perform MR angiography (details of MR procedure in chapter VI.1.4). Afterwards the patient was transferred back to the angiography unit and the catheter position was confirmed by X-ray. The chemotherapy (5 to 7 ml of Lipiodol (Lipiodol Ultra Fluide, Guerbet, Villepinte, France) - oily iodinated contrast agent and 50 mg Doxorubicin in 10 ml 0.9% NaCl) was applied *via* catheter or microcatheter in the therapy position. Then the catheters and sheath were removed and angio-seal closure system was applied. A native CT scan one day after the procedure was performed to determine the distribution of the lipiodol. Antiemetic (4 mg Ondansetron), analgesic (50 mg Pethidinhydrochloride) and corticosteroids (250 mg Prednisolon) were administered intravenously in 250 ml NaCl bolus prior to application of chemotherapy.

Workflow

As previously described (Chapter III.2, interventional MR scanners, **Figure 1**) the angiography suite and MR suite were separated by a 3.7 meters wide corridor and equipped with sliding doors between them. The patients were transferred from the angiography table to the MR unit and then moved over a rolling board on the MR table. The contrast agent injector with specially diluted Gadolinium- 1,4,7,10-tetraazacyclododecane-1,4,7,10- tetraacetic acid (Gd-DOTA) (0.5-10.0% in first group and 5.0% in second group) (Dotarem, Guerbet, Villepinte, France) were prepared before the procedure. The patient already draped in sterile fashion at the beginning of the procedure was covered with sterile drapes and then the MR coil was placed (eight channel body matrix coil, Siemens Medical, Erlangen, Germany). Sterile plastic tube with contrast agent was connected to the distal part of the catheter. After placing the headphones and emergency bell the MR examination proceeded. Localizers were used to plan the following sequences: two GE sequences (detailed description in the chapter VI.1.4) were performed one after another and the contrast agent was injected twice (once per sequence) *via* the catheter in the hepatic artery. The 3D volume interpolated GE (VIBE) was performed as the first sequence in 22 patients whereas in 27 patients SPGR (FLASH 3D) was performed as the first sequence. Duration times of every procedure-related event were collected and analyzed in order to determine the effectiveness and to optimize the workflow for the future iMRI approaches.

VI.1.4 MR imaging protocol

The spatial coverage of the whole liver was provided. All images were obtained using the eight channel body matrix coil (Siemens Medical, Erlangen, Germany). All sequences were performed in parallel imaging technique and integrated parallel acquisition technique GRAPPA (Generalized Autocalibrating Partially Parallel Acquisition) with factor 2 was used in every sequence. At first, the baseline imaging without contrast agent administration in 3D VIBE and SPGR FLASH 3D were performed. Then the contrast enhanced sequences were

performed in the following phases: arterial, portalvenous and late venous phase. The parameters of these sequences are summarized in **Table 14**. The contrast agent (Gadolinium DOTA, Dotarem, Guerbet, Villepinte, France) was applied automatically *via* catheter in the hepatic artery with 2 ml/s flow rate and followed by injection of 10 ml of 0,9% NaCl. The settings of the automated contrast agent injector are summarized in **Table 15**. In the first 9 patients and 13 examinations the contrast agent concentration varied from 0.5% to 10.0% in NaCl. The next 18 patients and 49 procedures followed the protocol with 5.0% dilution of gadolinium.

Sequence type	Slice orientation	TR ms	TE ms	FA (º)	Matrix (mm)	ST (mm)	GRAPPA*
VIBE	axial	3.22	1.24	12	320/160	2	2
Flash 3D	axial	2.78	1.07	25	512/112	1.6	2

Table 14 Sequence parameters.

* integrated parallel acquisition technique: GRAPPA; Generalized Autocalibrating Partially Parallel Acquisition

Contrast agent	Volume overall	Flow rate	Concentration	Time of injection
Gd-DOTA	20 ml	2 ml/s	0.5 - 10.0% - 13 procedures 5.0% - 49 procedures	10 seconds

Table 15 Contrast agent parameters.

VI.1.5 Qualitative analysis

Aim of this descriptive analysis was to estimate the optimal contrast agent concentration for the MR angiography during TACE. First 13 procedures in 9 patients were performed with different MR contrast agent concentrations (from 0.5% to 10.0%) applied *via* the catheter in the hepatic artery. These examinations served to estimate the optimal

concentration of applied Gd-DOTA for the best image quality. Two radiologist blinded to the contrast agent concentration evaluated all images independently in 13 first examinations using a dedicated questionnaire with four questions concerning image quality and gaining potential information due to i.a. transcatheter in MR angiography. The image quality questions are summarized in detail in the **Table 16**. The additional information as confirmation of complete tumor targeting, additional tumor vascularization from another branch, tumor depiction possible only in MRI due to inconclusive angiography, detection of new lesions with MR contrast enhancement (metastases/ high grade dysplastic nodules), were also evaluated.

The FLASH 3D and VIBE sequences with different concentrations of Gd-DOTA 0.5%, 1.0%, 1.5%, 2.5%, 3.0%, 5.0% and 10.0% were performed only in the arterial phase. Every sequence in every procedure was evaluated and placed in the scale from best to worst in the questionnaire. The scoring system is presented in the **Table 16**. Due to the low number of patients in this subgroup a statistical analysis of differences between two applied sequences was not performed.

Image quality question	Scoring for every question
1. Depiction of perfused liver segment	The very best one: 3 points
2. Depiction of tumor vs. perfused liver segment	The middle one: 2 points
3. Depiction of tumor vs. non perfused liver segment	The acceptable one: 1 point
4. Presence of catheter artifact in the vessels [yes/no]	Poor image quality: 0 points

Table 16 Scoring system for qualitative analysis.

VI.1.6 Quantitative analysis

Aim of this analysis was to determine image quality of obtained sequences in transcatheter intraprocedural MR angiography with application of 5.0% Gd-DOTA during TACE. For this purpose the quality parameters like SNR and CNR were evaluated. The comparison of SNR in the phase of maximal tumor enhancement, SNR of the whole tumor, SNR of the unenhanced liver and CNR of the tumor (maximum enhancement) to normal liver as well as CNR whole tumor to normal liver of the two applied GE sequences were performed using non-parametric Mann Whitney test (significance at P levels < 0.05). The follow up of the tumor enhancement in MR image was analyzed in 9 patients who underwent three or more consecutive TACE with i.a. transcatheter MR angiography. Signal parameters in 18 patients and 49 TACE procedures with i.a. transcatheter liver tumor perfusion in MR angiography were analyzed. Statistical tests were performed using the Version 5.03 of Graph Pad Prism software (GraphPad Software Inc. La Jolla, CA, USA). Benefits resulting from i.a. transcatheter contrast agent application in MR angiography during TACE namely: confirmation of complete tumor targeting, additional tumor vascularization from another branch, tumor depiction possible only in MRI due to inconclusive angiography, detection of new lesions with MR contrast enhancement (metastases/ high grade dysplastic nodules) were evaluated.

VI.1.6.1 Signal parameter assessment

The signal parameters were assessed in all examinations with 32-bit Osirix Imaging Software DICOM viewer, using region of interest (ROI) analysis.

Before obtaining contrast enhanced MR scans by VIBE and FLASH 3D sequences, an unenhanced scan of each sequence was performed twice for the subsequent subtraction and calculation of background noise. The standard deviation (SD) in ROI placed in the tumor (in the region of maximal enhancement as well as in the point of maximal axial tumor diameter) and liver parenchyma on subtracted unenhanced image were considered as an

image noise for the lesion and normal liver parenchyma. The ROI placed in the tumor and liver parenchyma on contrast enhanced images and their mean pixel values were considered as signal intensity (SI). The SI in the tumor was measured in the region of maximal enhancement as a mean value of three consecutive measurements. The SI was also obtained for the whole tumor and was measured in the place of maximal axial tumor diameter. The integrated parallel imaging technique used in our MR scanner was GRAPPA and the accelerator factor of 2 was applied. The "g" factor was not explicitly calculated due to complex coils sensitivity maps and noise correlation matrix, which were not available. The SNR and CNR were calculated as follows (62).

$$SNR\ region\ of\ max.\ tumor\ enhanc.=\dfrac{\sqrt{}}{\overline{}}$$

$$SNR\ whole\ tumor=\dfrac{\sqrt{}}{\overline{}}$$

$$SNR\ liver=\dfrac{\sqrt{}}{\overline{}}$$

$$CNR\ point\ of\ max.\ tumor\ enhanc./liver=\overline{}\ \dfrac{}{\overline{}\sqrt{}-\overline{}\sqrt{}}$$

$$CNR\ whole\ tumor/liver=\dfrac{}{\overline{}\sqrt{}-\sqrt{}\overline{}}$$

SI, Signal intensity; SD, Standard deviation

VI.2 Results

VI.2.1 Results of workflow analysis

Table 17 presents each event registered, their average duration in minutes (Mean ± SD), maximum and minimum values.

Events	Mean (± SD) (min.)	Max (min.)	Min (min.)
Access to the groin	7.55 (± 7.92)	30	2
Cannulation of the tumor vessel	42.22 (± 21.46)	110	6
Transfer to MRI suite	11.09 (± 6.86)	31	2
Time in MRI	15.78 (± 6.43)	40	7
Transfer to angiography suite	9.15 (± 6.35)	25	2
Cannulation after MRI (in case of another therapy position or catheter dislocation)	19.21 (± 22.21)	105	1
TACE	26.38 (± 17.46)	85	5

Table 17 Average duration of every event during TACE with i.a. transcatheter MR angiography.

A delay in transferring the patient from the angiography suite to the MRI area was observed in the 71.19% of the cases due to the occupation of the MRI by patients scheduled for a diagnostic MRI. The average waiting time before transferring the patient was of 20.68 (± 19.91) minutes with a maximum waiting time of 80 minutes.

Overall, the TACE procedure is divided in 3 blocks: a first part in the angiography suite, the second part in the MRI area and the third part describes the TACE procedure back in the angiography suite. **Table 18** shows the average, maximum and minimum times for each phase of the procedure.

Phase	Mean (± SD) (min.)	Max (min.)	Min (min.)
First: angiography	53.73 (± 24.35)	124	15
Second: MRI	28.22 (± 11.84)	80	7
Third: angiography	50.93 (± 26.32)	146	13

Table 18 Times recorded for every phase of the TACE with i.a. transcatheter MR angiography.

The times presented in **Table 18** do not take into account the waiting times for MRI in case of delay.

VI.2.2 Results of qualitative analysis: 5.0% as the optimal concentration of gadolinium in FLASH 3D and VIBE sequences

Results of qualitative analysis of two applied sequences are demonstrated in **Tables 19** and **20**. The optimal concentration allowing the best depiction of perfused liver segment as well as the best depiction of tumor versus perfused and non-perfused liver segment was 5.0% in both sequences used. The lower concentration of the contrast agent prohibited sharp tumor delineation, especially in large tumor masses. The 10.0% concentration did not allow good tumor delineation either, due to similar signal intensity of the tumor and surrounding liver tissue. Additional information gained by i.a. contrast agent application in MR allowed to avoid two incomplete tumor embolizations. In one patient one new lesion (second HCC) was discovered, which was not diagnosed by regular MRI after intravenous (i.v.) contrast enhanced MR scan. All additional information is summarized in **Table 21**.

Image quality question	Concentration of Gd-DOTA in FLASH 3D						
	0.5%	1.0%	1.5%	2.5%	3.0%	5.0%	10.0%
1. Depiction of perfused liver segment	0	5	0	4	0	13	0
2. Depiction of tumor vs. perfused liver segment	0	0	0	8	0	1	0
3. Depiction of tumor vs. non perfused liver segment	0	0	5	6	0	11	0
4. Presence of catheter artifact in the vessels [yes/no]	no	no	no	no	no	no	no
Points overall	0	5	0	18	0	25	5

Table 19 Different concentrations of Gd-DOTA during FLASH 3D sequence. The points were calculated by subjective judgment of two radiologists according to the scoring system (chapter VI.1.5).

Image quality question	Concentration of Gd-DOTA in VIBE						
	0.5%	1.0%	1.5%	2.5%	3.0%	5.0%	10.0%
1. Depiction of perfused liver segment	0	0	0	0	0	3	2
2. Depiction of tumor vs. perfused liver segment	0	0	0	0	0	11	5
3. Depiction of tumor vs. non perfused tumor segment	0	0	0	0	0	11	1
4. Presence of catheter artifact in the vessels [yes/no]	no	no	no	no	no	no	no
Points overall	0	0	0	0	0	25	8

Table 20 Different concentrations of Gd-DOTA during VIBE sequence. The points were calculated by subjective judgment of two radiologists according to the scoring system (chapter VI.1.5).

Additional information due to intraprocedural MRI with intraarterially administerd contrast agent	Number of examinations N = 13
1. Confirmation of complete tumor targeting (primary uncorrected catheter position)	11 examinations (85%)
2. Additional tumor vascularization from another branch	2 examinations (15%)
3. Delineation of necrotic areas in the tumor	6 examinations* (46%)
4. Tumor depiction only in MRI, inconclusive angiography	3 examinations* (23%)
5. Detection of new lesions with MR contrast enhancement (metastases/ high grade dysplastic nodules)	1 examination* (8%)

Table 21 Additional information due to i.a. transcatheter MR angiography during TACE in first 13 examinations.

*- delineation of necrotic tumor areas as well as tumor depiction only in MRI and detection of new lesions can occur simultaneously in more than 1 procedure.

VI.2.3 Results of quantitative analysis

SNR MEASUREMENTS:

VIBE yields higher SNR in the region of maximal tumor enhancement compared to FLASH 3D

SNR tumor measured in the region of maximal tumor enhancement was higher in images acquired by VIBE sequence; this was true for arterial, portalvenous and late venous phases (p values 0.02, 0.01 and 0.002, respectively). The results are demonstrated in in **Figures 12 - 14**.
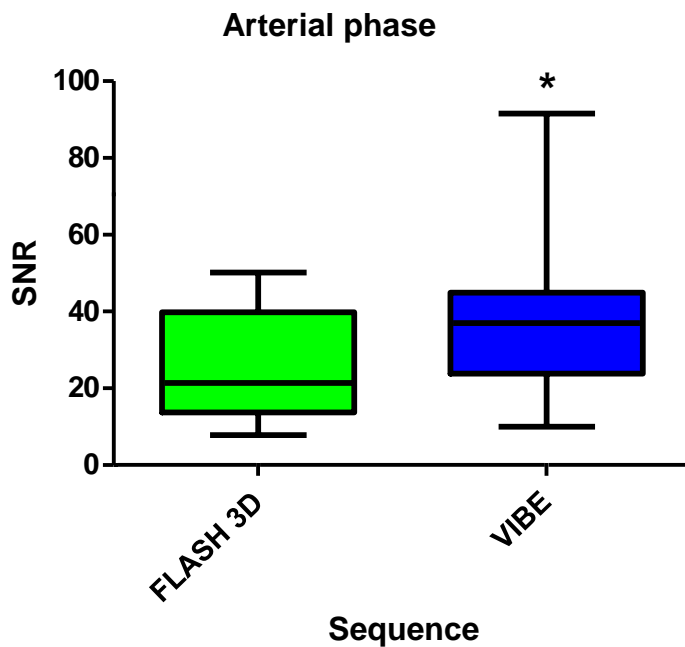
Figure 12 SNR in the region of maximal tumor enhancement in FLASH 3D in arterial phase (median: 21.36, min: 7.79, max: 50.11) and VIBE sequence (median: 36.96, min: 9.92, max: 91.54) in the arterial phase. *p < 0.05

Portalvenous phase
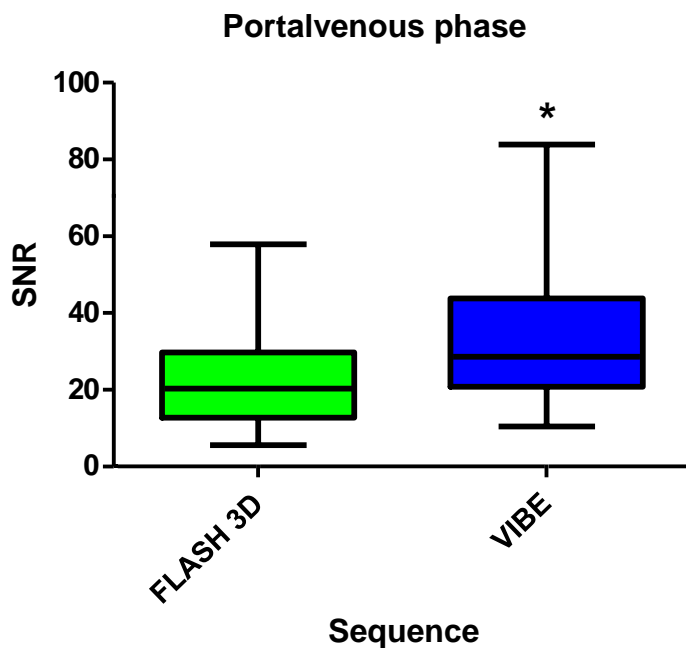
Figure 13 SNR in the region of maximal tumor enhancement in FLASH 3D in portalvenous phase (median: 20.25, min: 5.50, max: 57.87) and VIBE sequence (median: 28.59, min: 10.48, max: 83.89) in portalvenous phase.*p < 0.05
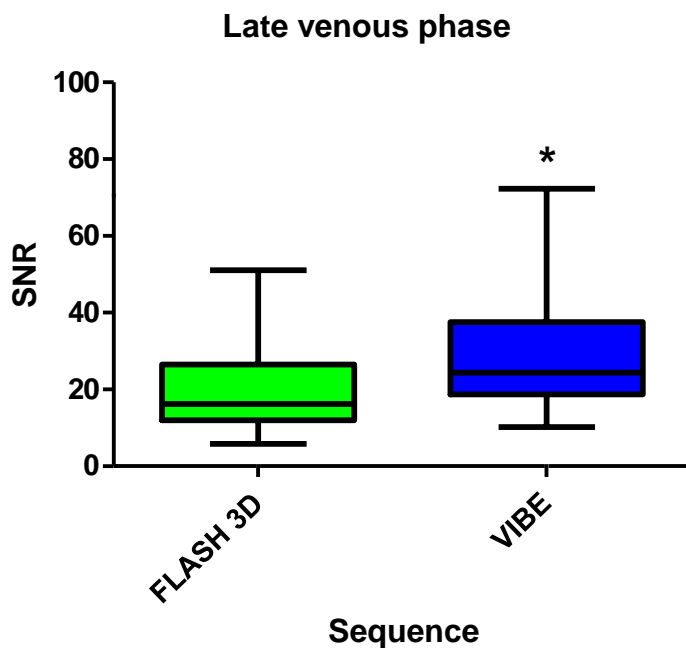
Late venous phase

Figure 14 SNR in point of maximal tumor enhancement in FLASH 3D in late venous phase (median: 16.19, min: 5.83, max: 51.03) and VIBE sequence (median: 24.37, min: 10.21, max: 72.28) in the late venous phase. *p < 0.05

VIBE yields higher SNR compared to FLASH 3D measured in the whole tumor

The assessment of SNR in the whole tumor (defined as maximal axial diameter, including perfused and not perfused necrotic areas) in the arterial, portalvenous and late venous phase demonstrated that the SNR of the VIBE sequence is higher compared to FLASH 3D sequence (p values: 0.01, 0.005 and 0.0004, respectively). The results are demonstrated in **Figures 15 - 17**.
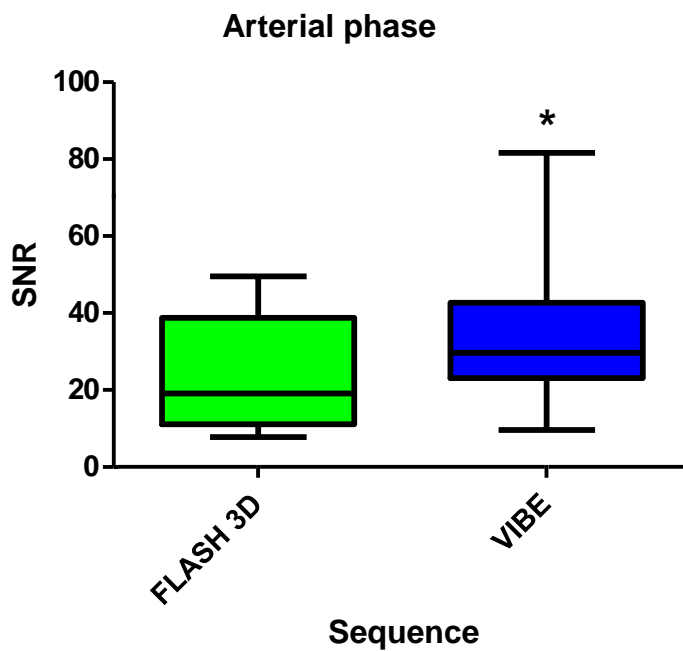
Figure 15 SNR in the whole tumor in FLASH 3D in arterial phase (median: 19.14, min: 7.80, max: 49.57) and VIBE sequence (median: 29.73, min: 9.61, max: 81.61) in the arterial phase. *p < 0.05

Portalvenous phase
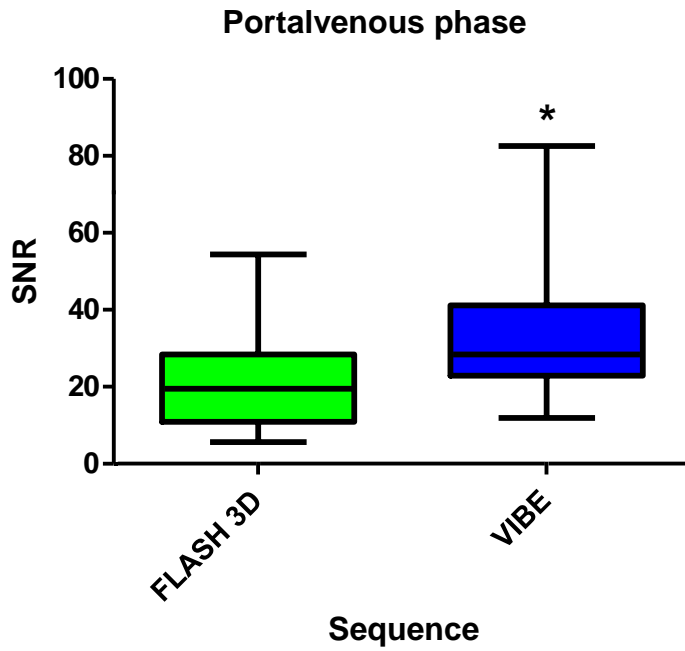
Figure 16 SNR in the whole tumor in FLASH 3D in portalvenous phase (median: 19.45, min: 5.66, max: 54.39) and VIBE sequence (median: 28.34, min: 11.85, max: 82.53) in the portalvenous phase. *p < 0.05
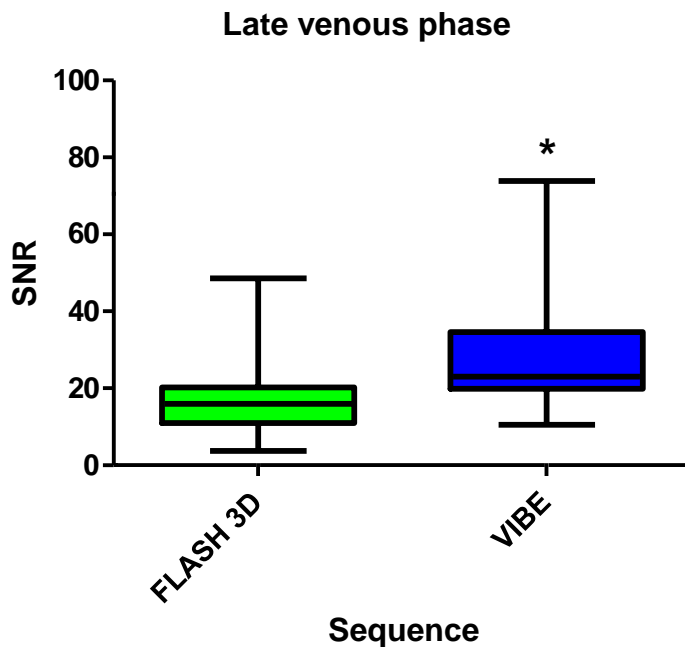
Late venous phase

Figure 17 SNR in the whole tumor in FLASH 3D in late venous phase (median: 15.95, min: 3.71, max: 48.57) and VIBE sequence (median: 23.03, min: 10.54, max: 73.91) in the late venous phase. *p < 0.05

VIBE yields higher SNR in the unenhanced liver compared to FLASH 3D

The SNR in unenhanced liver revealed significant differences between FLASH 3D and VIBE sequences in all applied phases with $p < 0.0001$, yielding a higher SNR for the VIBE sequence. The results are demonstrated in **Figures 18 - 20**.
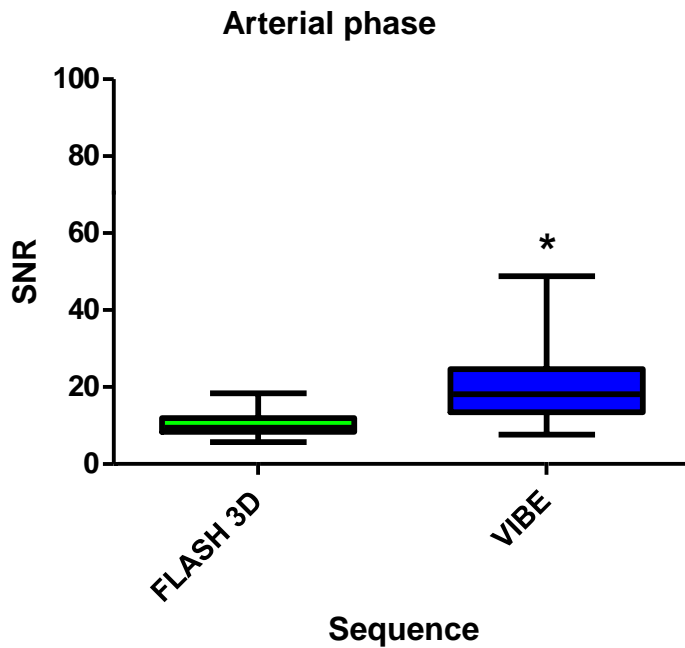
Figure 18 SNR in the liver in FLASH 3D in arterial phase (median: 9.48, min: 5.72, max: 18.34) and VIBE sequence (median: 18.16, min: 7.61, max: 48.76) in the arterial phase. *$p < 0.05$

Portalvenous phase
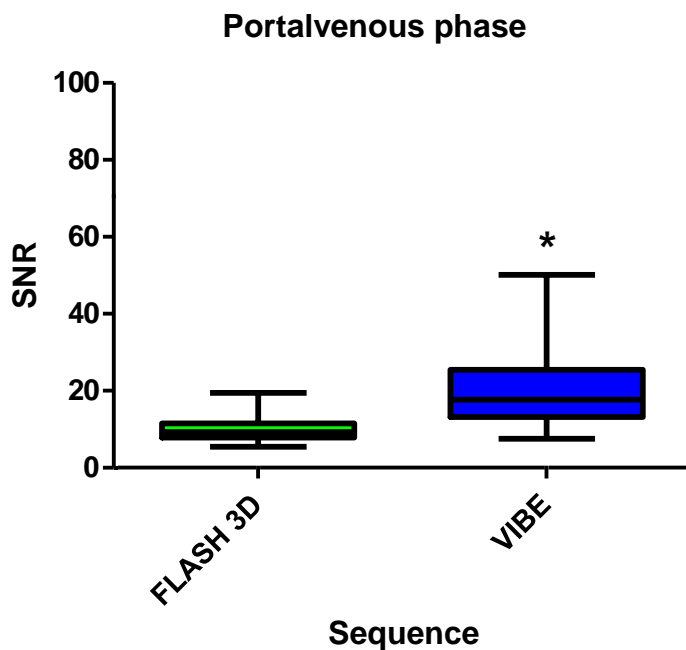
Figure 19 SNR in the liver in FLASH 3D in portalvenous phase (median: 9.28, min: 5.45, max: 19,43) and VIBE sequence (median: 17.74, min: 7.58, max: 50.12) in the portalvenous phase. *p < 0.05
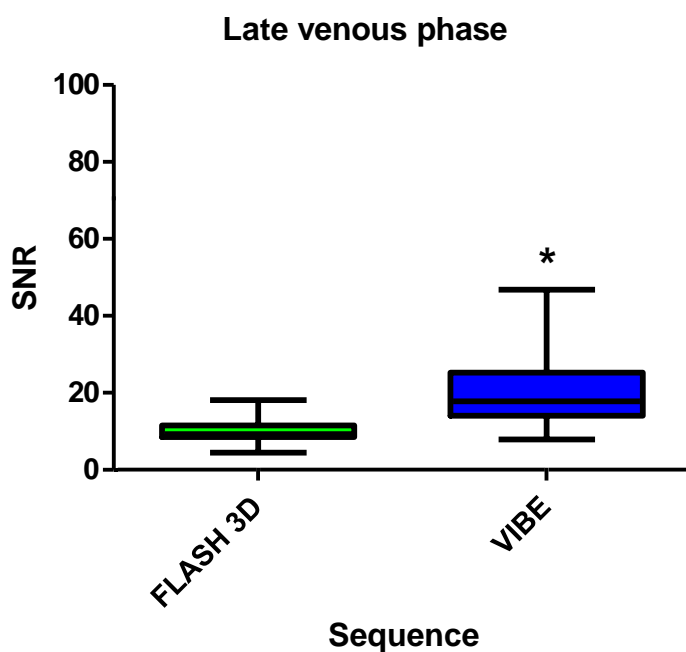
Late venous phase

Figure 20 SNR in the liver in FLASH 3D in late venous phase (median: 9.27, min: 4.47, max: 18.12) and VIBE sequence (median: 17.75, min: 7.89, max: 46.81) in the late venous phase. *p < 0.05

Comparison of SNR between the region of maximal tumor enhancement and the whole tumor yielded no statistically significant differences either in VIBE or in FLASH 3D sequence

SNR comparison between the region of maximal tumor enhancement and the whole tumor (defined as maximal axial diameter) showed no statistical differences. The comparison was conducted separately for FLASH 3D and VIBE sequence. In FLASH 3D sequence, the p values for arterial phase equaled 0.54, for portalvenous phase 0.65 and for late venous phase 0.64. In VIBE sequence, the p values for arterial phase equaled 0.39, for portalvenous phase 0.89 and for late venous phase 0.84. The results are presented in **Tables 22 and 23**.

VIBE sequence	SNR in the region of max. tumor enhancement	SNR in the whole tumor
Phase		
Arterial	36.96 [9.92 - 91.54]	29.73 [9.61 - 81.61]
Portalvenous	28.59 [10.48 - 83.89]	28.34 [11.85 - 82.53]
Late venous	24.37 [10.21 - 72.28]	23.03 [10.54 - 73.91]

Table 22 Results of SNR (region of max. tumor enhancement versus whole tumor) in VIBE sequence. SNR values are presented as medians and ranges.

FLASH 3D sequence	SNR in the region of max. tumor enhancement	SNR in the whole tumor
Phase		
Arterial	21.36 [7.79 - 50.11]	19.14 [7.80 - 49.57]
Portalvenous	20.25 [5.50 - 57.87]	19.45 [5.66 - 54.39]
Late venous	16.19 [5.83 - 51.03]	15.95 [3.71 - 48.57]

Table 23 Results of SNR (region of max. tumor enhancement versus whole tumor) in FLASH 3D sequence. SNR values are presented as medians and ranges.

CNR MEASUREMENTS:

Contrast to noise ratio in the region of maximal tumor enhancement/liver reveals no statistically significant differences between VIBE and FLASH 3D sequences

The CNR between the region of maximal tumor enhancement and tumor-free liver demonstrated no significant differences between FLASH 3D and VIBE sequences in any of the applied phases (p = 0.51 for arterial phase, p = 1.0 for portalvenous phase and p = 0.69 for late phase). The results are given in **Table 24**.

Phase	CNR in region of maximal tumor enhancement/liver	
	VIBE	FLASH 3D
Arterial	16.11 [0.84 - 65.23]	10.96 [0.65 - 41.35]
Portalvenous	9.86 [0.50 - 54.65]	11.96 [0.08 - 38.43]
Late venous	6.30 [0.46 - 54.10]	7.03 [0.48 - 32.90]

Table 24 Results of CNR (region of max. tumor enhancement versus tumor-free liver) in VIBE and FLASH 3D sequences. CNR values are presented as medians and ranges.

Contrast to noise ratio of the whole tumor/liver reveals no statistically significant differences between VIBE and FLASH 3D sequences

The CNR between the whole tumor enhancement (defined as maximal axial diameter) and tumor-free liver demonstrated no significant differences between FLASH 3D and VIBE sequences in none of the applied phases (p = 0.60 for arterial phase, p = 0.63 for portalvenous phase and p = 0.94 for late phase). The results are presented in **Table 25**.

Phase	CNR in the whole tumor/liver	
	VIBE	FLASH 3D
Arterial	14.74 [0.21 - 55.30]	10.41 [0.72 - 40.81]
Portalvenous	8.94 [1.04 - 58.99]	10.57 [0.25 - 36.22]
Late venous	6.85 [0.15 - 51.07]	6.77 [0.97 - 30.44]

Table 25 Results of CNR (whole tumor versus tumor-free liver) in all phases in VIBE and FLASH 3D sequences. CNR values are presented as medians and ranges.

Comparison between CNR of the region of maximal tumor enhancement/tumor-free liver and CNR of the in whole tumor/tumor-free liver reveals no statistically significant differences neither in VIBE nor in FLASH 3D sequence

Comparison of CNR values calculated for the region of maximal tumor enhancement and the whole tumor each time correlated to the tumor-free liver demonstrated no statistically significant difference. The calculation was done within one sequence and identical perfusion phases. In FLASH 3D sequence, the p values for arterial phase equaled 0.62, for portalvenous phase 0.67 and for late venous phase 0.83. In VIBE sequence, the p values for arterial phase equaled 0.51, for portalvenous phase 0.97 and for late venous phase 0.88. The results are presented in **Tables 26** and **27**.

VIBE sequence	CNR in the region of max. tumor enhancement/liver	CNR in the whole tumor/liver
Phase		
Arterial	16.11 [0.84 - 65.23]	14.74 [0.21 - 55.30]
Portalvenous	9.86 [0.50 - 54.65]	8.94 [1.04 - 58.99]
Late venous	6.30 [0.46 - 54.10]	6.85 [0.15 - 51.07]

Table 26 Results of CNR (region of max. tumor enhancement versus whole tumor) in VIBE sequence. CNR values are presented as medians and ranges.

FLASH 3D sequence	CNR in the region of max. tumor enhancement/liver	CNR in the whole tumor/liver
Phase		
Arterial	10.96 [0.65 - 41.35]	10.41 [0.72 - 40.81]
Portalvenous	11.96 [0.08 - 38.43]	10.57 [0.25 - 36.22]
Late venous	7.03 [0.48 - 32.90]	6.77 [0.97 - 30.44]

Table 27 Results of CNR (region of max. tumor enhancement versus whole tumor) in FLASH 3D sequence. CNR values are presented as medians and ranges.

VI.2.4 Follow up and MR angiography benefits

Follow up of SNR in the whole tumor (defined as maximal axial diameter) demonstrates its decrease in consecutive procedures

The follow up of the tumor enhancement in MR image was analyzed in those patients, who underwent three or more TACE with i.a. transcatheter MR angiography. This was the case in nine patients. Three patients underwent four consecutive TACE procedures and in this group SNR in the whole tumor was decreasing from one procedure to the next. In one patient however the SNR decreased after the first TACE and then increased in the next two procedures. Six patients underwent three consecutive TACE procedures. In this group of patients the SNR of the whole tumor were decreasing or remained equal. Detailed characteristics of the patients, their lesions and procedures are presented in **Table 28**. The results of the analysis are presented in **Figures 21** and **Figure 22.** No statistical calculations were done due to the small number of patients available for the analysis.

Patient's number	Prior TACE treatments before inclusion into the study	HCC characteristics in the beginning of the TACE therapy at the point of inclusion in the study	Group (I: four consecutive TACE procedures, II: three consecutive TACE procedures)
1	1 TACE	Multilocular, bilobar (two nodules)	I
2	2 TACE	Multilocular (two nodules in right liver lobe)	I
3	none	Unilocular in right liver lobe	I
4	3 TACE	Unilocular in watershed distribution in the right liver lobe	II
5	2 TACE	Unilocular in the left liver lobe	II
6	None	Multilocular lesion in the right liver lobe	II
7	None	Unilocular in right liver lobe and multiple dysplastic nodules	II
8	2 TACE	Multilocular, bilobar (two in right and one in left liver lobe)	II
9	None	Unilocular in left liver lobe	II

Table 28 Characteristics of patients and their HCC lesions who underwent three or more consecutive TACE procedures. Patient's numbers are not consistent with the order of entry into the study.
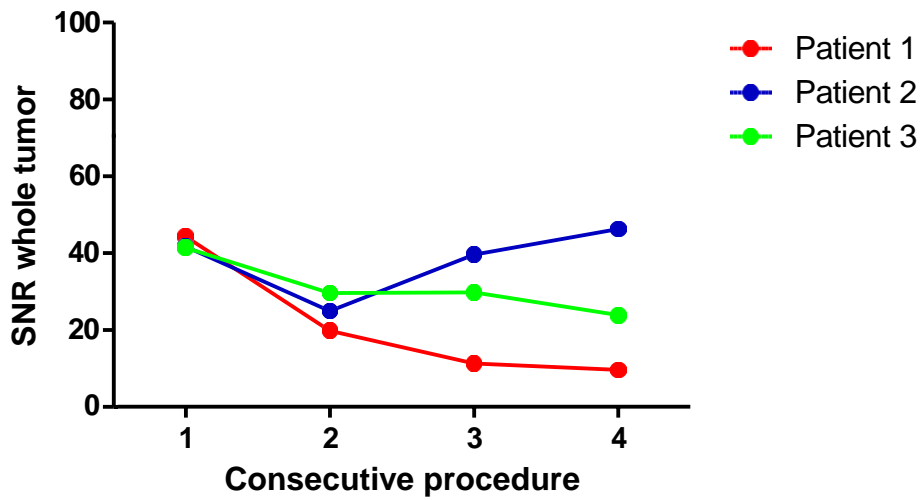
Figure 21 SNR of the whole tumor in three patients who underwent four consecutive TACE procedures.
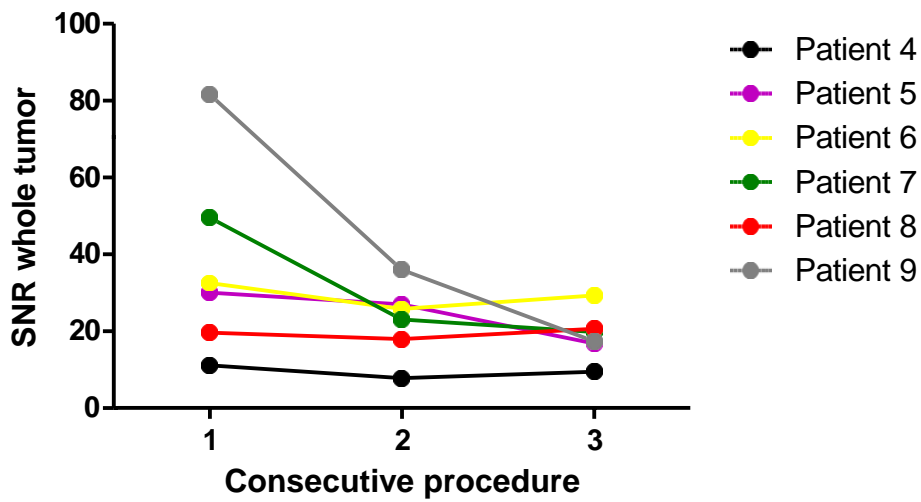
Figure 22 SNR of the whole tumor in six patients who underwent three consecutive TACE procedures.

Additional information gained by transcatheter intraarterial liver tumor perfusion in MR angiography during transarterial chemoembolization

Additional information obtained during transcatheter intaarterial MR angiography performed in 49 procedures is in detail summarized in **Table 29.** In 86% of procedures (n = 42) the primary catheter position was judged to be correct due to observed entire tumor perfusion in MRI. The necrotic tumor areas were demarcated in 29 among of 42 examinations, mostly in patients with multiple TACE procedures performed. In 7 examinations (14%) the primary catheter position had to be revised to achieve better tumor targeting: in four procedures as consequence of additional arteries supplying the tumor (8%), in three procedures as consequence of suboptimal primary catheter position (2%) or contrast enhancement of the gallbladder (4%). New lesions (HCC-metastases or high grade dysplastic nodules) were discovered in three MR TACE procedures; these were not included in the group with suboptimal primary catheter position. The example of a difficult tumor location is presented in **Figures 23 - 26.** In this patient the tumor enhancement was readily identified under fluoroscopy after contrast agent application via the left hepatic artery (**Figure 23**). The additional vascularization from the branches of the right hepatic artery could not be detected by DSA. Contrast enhanced FLASH 3D sequence (**Figure 24** and **25)** demonstrated that approximately 2/3 of the tumor was supplied by the left hepatic artery and 1/3 by the right hepatic artery. **Figure 26** is the native CT scan showing complete tumor targeting after TACE with lipiodol being performed via both hepatic arteries. The examples of a potentially malignant new HCC lesion are presented in **Figures 27-30**.

Additional information due to intraprocedural MRI with intraarterially administered contrast agent	Number of examinations N = 49
1. Confirmation of complete tumor targeting (primary uncorrected catheter position)	42 examinations (86%)
2. Additional tumor vascularization from another branch	4 examinations (8%)
3. Suboptimal therapy position (Gallbladder enhancement, false liver segment)	3 examinations (6%)
4. Delineation of necrotic areas in the tumor	29 examinations* (59%)
5. Tumor depiction only in MRI, inconclusive angiography	3 examinations* (6%)
6. Detection of new lesions with MR contrast enhancement (metastases/ high grade dysplastic nodules)	3 examinations* (6%)

Table 27 Benefits of MR angiography in 18 patients and all together 49 examinations.

*Delineation of necrotic tumor areas as well as tumor depiction only in MRI and detection of new lesions can occur simultaneously in more than 1 procedure.
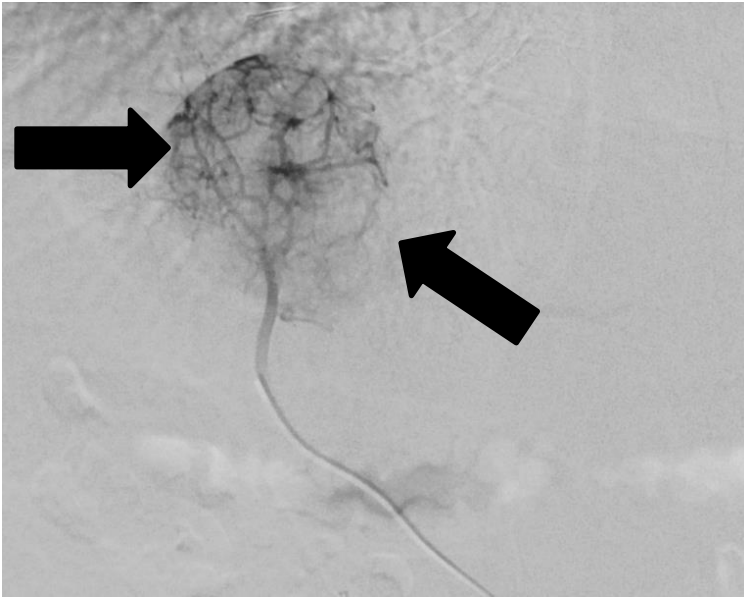
Figure 23
DSA image of the HCC in liver segment 4 (arrows) after injection of iodized contrast agent *via* the left hepatic artery.
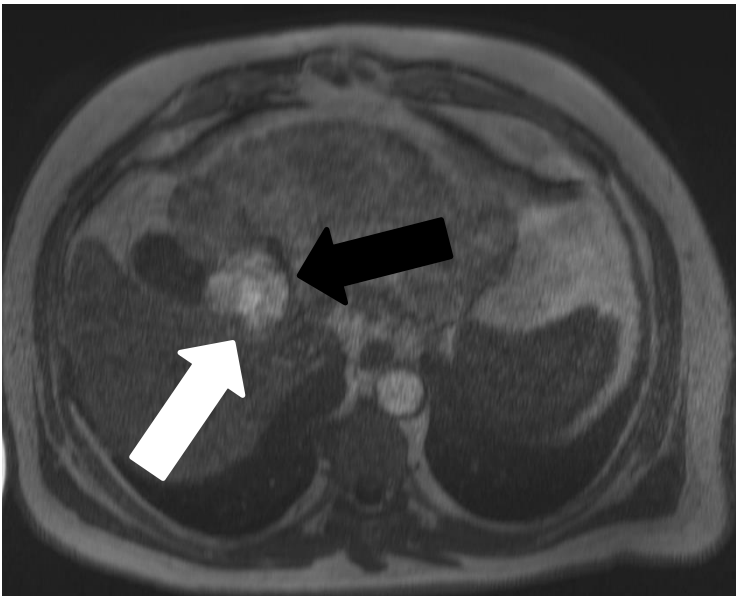
Figure 24
HCC in liver segment 4 (black arrow) depicted during a FLASH 3D after application of Gd-DOTA *via* catheter in the left hepatic artery, not enhanced rim of the tumor (white arrow) as hint for additional arterial supply from another vessel.
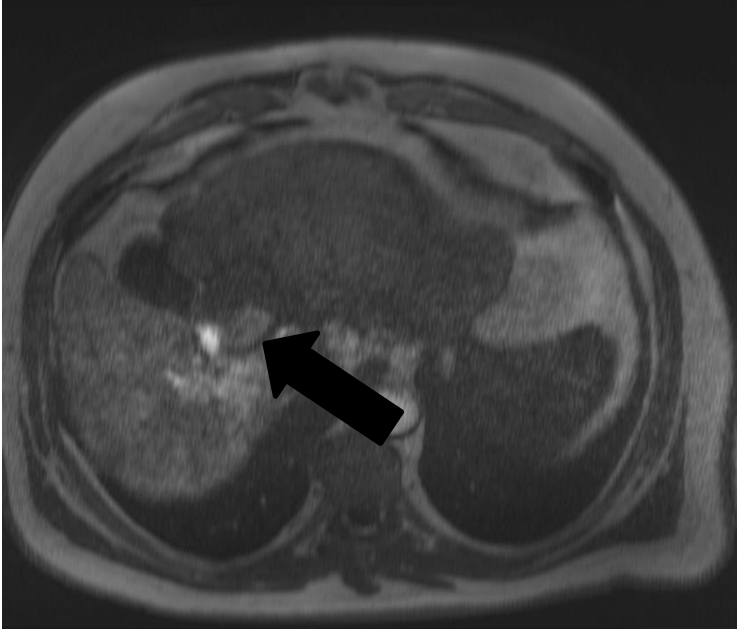
Figure 25
HCC in liver segment 4 depicted during a FLASH 3D after application of Gd-DOTA *via* catheter in the right hepatic artery: previously non enhanced rim of the tumor demonstrates contrast enhancement (black arrow).
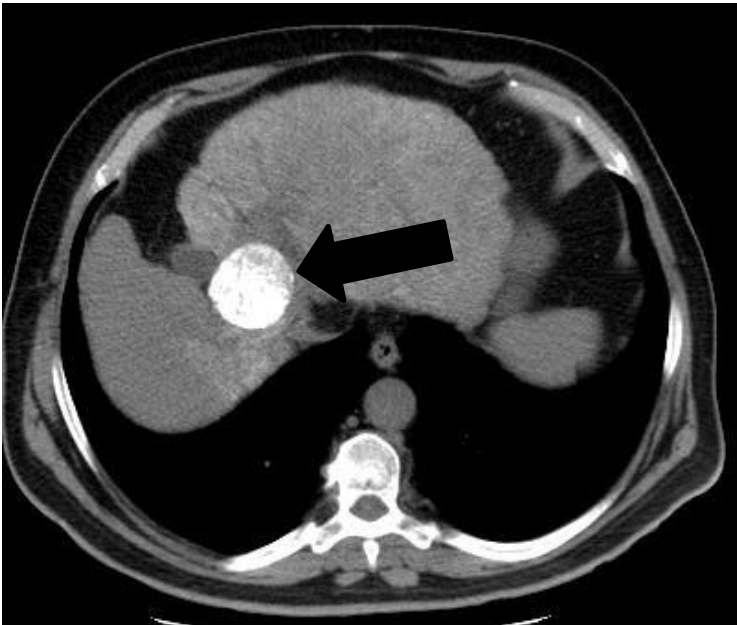
Figure 26
Lipiodol retained within the HCC in liver segment 4 (black arrow) on a native CT scan one day after TACE with application of chemotherapy and lipiodol via both hepatic arteries.

Figure 27
New HCC lesion in segment 6 of the liver (black arrow) after intraarterial contrast agent application in the arterial phase.
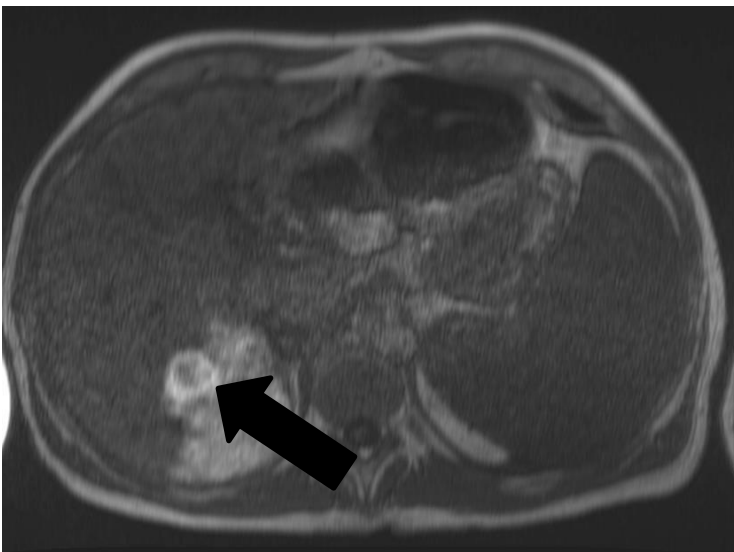
Figure 28
New HCC lesion in segment 6 of the liver (black arrow) after intraarterial contrast agent application in the portal venous phase with washout phenomenon.
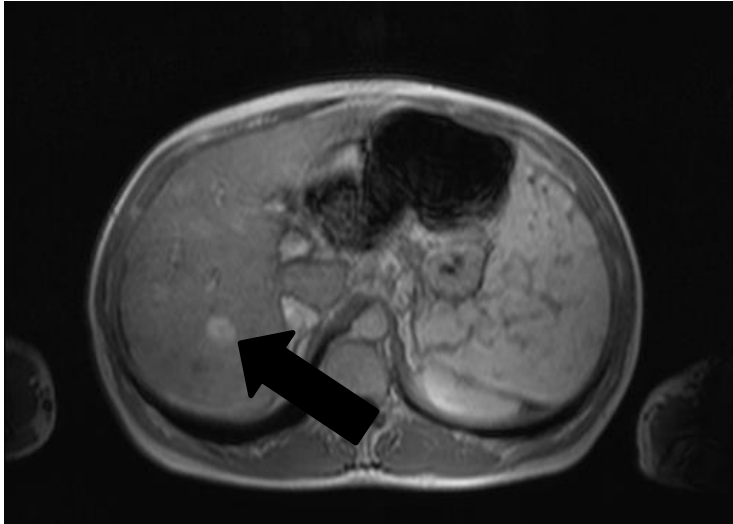
Figure 29
The same HCC lesion as in Figures 28-29 in segment 6 of the liver (black arrow) after i.v. contrast agent application in regular MR scan in the arterial phase.
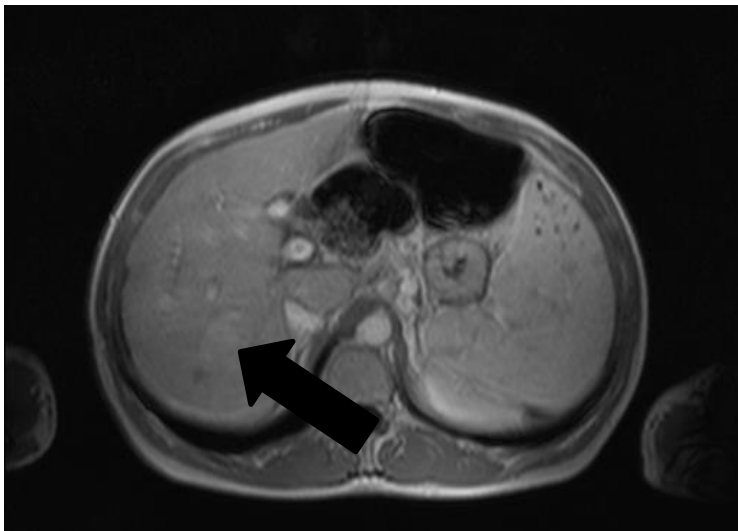
Figure 30
The same HCC lesion as in Figures 28-29 in segment 6 of the liver (black arrow) after i.v. contrast agent application in regular MR scan in the portal venous phase. Please note the differences between washout phenomenon after the intraarterial and i.v. contrast application.

VII. DISCUSSION

VII.1 PART 1: MR safety of interventional instruments and their validation in vascular models

According to FDA (Food and Drug Administration) or CEN (European Committee of Standardization), as well as ISO (International Organization of Standardization) MR safety and compatibility are recognized as a relevant issue in production of medical instruments. Despite the fact that standardized methods of testing medical devices already exist (i.e ASTM: American Society of Testing and Materials), the number of MR safe devices on the market is sparse. Several investigations in animal models and involving limited cohorts of patients (44, 72) demonstrated the feasibility and effectiveness of glass fibers embedded in epoxy resin, organic polymers like PEEK or fiberplastics. A newly published study by *Bell et al.* (4) describes passive and active navigation possibilities of a MR compatible Kevlar-made GW. The diameter of this wire (1.4 mm") is however too large for standard catheters so its potential practical application possibilities are limited. Three German companies (Epflex, Dettingen, MaRVis, Aachen, and Andramed, Reutlingen) already offer the prototypes of MR compatible GWs. However by the time of our study none of them received the CE marking (Conformité Européenne) hence their use in patients was not allowed and further studies were necessary. Epflex and MaRVis GWs, the only ones available to us, present similar lengths and diameters compared to standard GWs and are in the preclinical research phase. These novel GWs prototypes were employed in the first part of the study.

Heating experiments with standard and MR compatible guidewires

The first prototypes of an Epflex GW were already tested in animal trials (40, 41), however their potential heating in 1.5 T MR scanner has not been investigated. Therefore, in the first experiment with an aorta phantom the potential heating of the Epflex GW prototype was compared with the regular nitinol GW. It is already well documented that nitinol-based

wires exposed to radiofrequency energy during an MR experiments can produce heating due to their conductive properties (13, 42, 56). Our results confirm that the nitinol GW demonstrated the temperature elevation in GE sequences. Therefore we used this GW as a reference in our heating measurements. In our study we focused on imitating the scenario of the MR guided endovascular intervention. Because the GW position depends on the patients anatomy and the type of the endovascular procedure, we put the phantom in two different positions in the scanner: in isocenter and as far off-center as possible. The first position could imitate the interventions performed on the aorta, renal arteries or vena cava. The latter one is mostly used in approaches on peripheral femoral or tibial vessels. Furthermore, positioning the GW in off-center position induces more likely heating due to applied radiofrequency pulses and thus SAR levels. Minor increase of temperature of nitinol GW, like in isocenter position, should not injure the thick vessel wall of the aorta. The resonance phenomenon occurrence is however difficult to predict since it depends also on many environmental factors (for example body mass or temperature of the patient) and sudden, unexpected temperature increase of nitinol-based GW has to be taken into consideration. Moreover the temperature is more likely to increase in occluded or stenotic vessels and such scenario is to expect in patients with atherosclerosis. As demonstrated by Konings (42) at al. the presence of stenosis can increase the RF heating and may result in elevation of the GW temperature to 80°C. In our study, the nitinol GW in the off-center position of the aorta phantom in the scanner demonstrated substantial increase of the temperature of 9.6° for bSSFP and of 13° for SPGR sequence. It has to be taken into account that the first sequence was run only for 60 seconds and considering the steep increase and shape of the curve (**Figure 4**), the temperature probably would most likely increase even more with longer sequence duration. Epflex prototype GW minor temperature elevation of 0.1 - 0.4°C in both experiments is comparable with the temperature elevation of the reference probe attached to the MR table and was in the range of measurement variations. A single measurement point at the tip of the both GWs and lack of human shaped phantom were minor drawbacks of the

study. Especially the latter one is important because the size of the object in the MR field influences the B0 (static magnetic) and B1 (RF induced) fields. These limitations however were overcome in the next study with Thiel-embalmed human cadaver.

The next investigation on Thiel-embalmed cadaver was performed to mimic the conductivity of the human body. In this study it was possible to simulate the liquid flow in the left femoral artery with 0.9% saline solution, which has also similar conductivity to the human blood. The GW in the MR field acts like dipole antenna and electric currents translocate along the wire forming standing waves (42). This resonance phenomenon is dependent on the length of the GW and its position in MR field (42). The length of the GW determines if the waves can be reflected by the ends of such wire (42). Of note, 23 cm is the shortest GW length capable of producing resonance phenomena at 64 megahertz (MHz) in 1.5 T (48). Hence our standard nitinol GW with 150 cm was long enough to induce heating during MR measurements. In order to find and induce such resonance, we changed the GW position in MR field by retracting the GW 2 cm every 10 seconds. The retraction did not influence the temperature of nitinol GW by more than 2°. Even long scan times did not influence the temperature. In such scenario the saline flow also did not demonstrate any "cooling effect". In one previous study (13) it was demonstrated that sparks were produced when the GW end touched the bare animal skin. We were not able to replicate this observation in our experiment despite touching the skin of the cadaver, probably due to the resonance conditions. Limitations of the study include the single measurement point at the distal tip of the GW. The placement of such wire with the probe causes however extreme technical difficulties and has to be performed very carefully in order not to harm the cadaver vessel.

Artifact size of a new MR compatible guidewire prototype depends on time to echo (TE) under gradient echo sequences

These experiments were conducted with a novel MR compatible GW from MaRVis Company. The GW we used was in the phase of preclinical experiments at the time of the

study and tests of its passive visualization in a 1.5 T scanner was desirable. In the MaRVis GW iron markers are incorporated into the shaft of the wire and its depiction is based on their susceptibility artifacts. The artifacts size depends strongly on the type of the sequence. Spin echo (SE) sequences are prone to cause fewer artifacts than GE sequences (45, 47). In our experiment we chose the SPGR sequence (FLASH) since this sequence can be used for near real time imaging applied in MR guided procedures. Minimizing the echo time, increasing matrix and the slice thickness play a role in decreasing the susceptibility artifacts (60). The artifact size is important when performing interventional endovascular procedures especially in vessels of smaller caliber. Using a TE of 10 or 20 ms the tip marker of the wire was no longer distinguishable from the other markers and its artifact obscured the whole renal artery. This was true for both tested GW types (flexible and stiff one). In our investigation the GWs were also depicted in the aorta lumen, which had an inner diameter of 2.5 cm. In this case the artifacts were also present, but due to the larger vessel lumen, the wire was clearly visible in the aorta and did not mask the vessel walls. We confirmed that with shorter echo times the small-sized susceptibility artifacts allowed good depiction of the device inside the 5 mm lumen vessel, rendering the sequence with the lowest TE of 1.07 ms the most suitable for depicting the MaRVis GW.

Passive visualization of catheters in a vascular model

The endovascular devices, like catheters, pose specific features as elasticity, kinking resistance, radiopacity and differently shaped tips. Metal mesh from stainless steel (braiding) contributes to the rigidity and detectability by fluoroscopy. As explained before (Chapter III.4.2) this metal grid may also contribute to potential excessive heating during MR imaging. It is difficult to predict which catheter or what part of it is coveredd with the mentioned metal and how it will influence the magnetic field, since this information is mostly not available on the vendor website or instruction manual. On this account we have tested the catheters that are most commonly used in our angiography suite. Two phantoms, one purchased and

founded by the IIIOS project, were used. In the first phantom, where the catheters were inserted into a glass-made aorta, almost the entire shafts of the catheters could be explored and evaluated. The vessel phantom of the left lower extremity (Elastrat, Geneva, Switzerland) enabled the "closer look" at the catheter tips in good resolution. The catheters used in the clinical part of the study and considered MR safe showed no artifact during MRI. Catheters with metal components that are hazardous for the patient due to potential RF heating, were identified by susceptibility artifacts and on this account no longer taken into consideration during clinical part. Catheters with the hydrophilic layer (Terumo, Tokyo, Japan) demonstrated no metal mesh and no artifacts. They are not always the first choice during regular TACE procedures due to their softer shaft and potential instability. These features however facilitated their introduction into hepatic arteries without causing vessel spasms. Other instruments like intravascular sheaths were also tested in the MR environment, their length (i.e., 10 cm) however is considered not hazardous to present resonant effects (76) even in off center position in the scanner. According to antenna theory (33, 48) a shortest wire length acquired for resonance at 64 MHz corresponding to main magnetic field of 1.5 T is 23 cm. Furthermore, the introducer sheaths contained no metallic parts.

VII.2 PART 2: Evaluation of liver tumor perfusion by intraarterial transcatheter magnetic resonance angiography during transarterial chemoembolization in patients with hepatocellular carcinoma

Depending on the stage of the disease, TACE can be considered either as palliative or bridging therapy before liver transplantation, since it can reduce the tumor size (21). Indeed, the previous study of *Takayasu et al.* (68) conducted in over 8,000 patients treated with TACE demonstrated that median survival rate was 34 months in good responders. Another investigation conducted in 104 HCC patients revealed even higher median survival rates of 48.6 months (14). Delivery of the chemoembolic agents into the entire HCC is the main goal of TACE and is one of the main factors underlying the efficacy of this procedure (46). Concerning the good life expectancy, the best achievable tumor targeting is desirable. According to the literature (29, 47, 75) integrating MR into TACE enables monitoring the therapy and helps to determine the optimal catheter position. Our patient cohort encompasses 62 TACE procedures combined with MR imaging is to date the largest reported in the literature. During our prospective study we performed several analysis in order to optimize and evaluate the possible benefits of MRI for depiction of i.a. liver tumor perfusion during TACE.

Workflow

TACE, which is performed under fluoroscopy control, consists of several different steps and in our study was additionally complemented by MR imaging. Standard MR examination times depend on the examined anatomy and the sequences used and take approximately 30 to 60 minutes. To minimize the prolongation of the TACE procedure we performed only two diagnostic MRI sequences. We observed, that the "bottleneck" of the procedure was however not the MR scanning itself, but the waiting time for the MR scanner, when the catheter was placed in the therapy position. Although TACE patients were always a priori scheduled for MR examination, an accurate start time of the procedure was difficult to

predict since the cannulation of the tumor-supplying vessel under fluoroscopy is different in every TACE. Data analysis revealed that an average MR scan time was 15 minutes. In one case the scanning time was prolonged to 40 minutes due to a software error, which has to be taken into consideration when planning future procedures. In conclusion, MR imaging integrated into TACE prolonged the regular procedure time of about 35 minutes. The waiting period directly before the MR examination may be eliminated in centers with MR scanner destined for interventional procedures only. The combination of TACE with intraprocedural MRI is however troublesome in the every-day routine. This might be further aggravated by emergency cases requiring an MR examination. Consequently, the patients have to wait with the inserted sheath and catheter outside the MR scanner, what can potentially increase the risk of infection. This drawback on the other hand is outweighing by the benefits of the procedure like detection and correction of suboptimal catheter positions. Of note, no procedure-related complications were observed.

Qualitative analysis

The sequences applied in the evaluation of tumor perfusion in MR were both T1 weighted GE sequences. Both sequences are regularly used for MR examinations after i.v. contrast agent application. The gadolinium concentrations and flow rates applied i.a. were different from the regular i.v. applications and were tailored to the caliber of the vessel. In our investigation the flow rate of contrast agent was always 2 ml/s to avoid vessel injury and backwards flow of the contrast agent. The dilution of contrast agent of 20.0% reported by other authors (29) was according to our analysis too high for the selective catheter position in the liver. Although the gadolinium is a safe option even in patients with impaired renal function (55) its amount should be reasonably restricted. Several contrast agent concentrations were tested in the first patients subgroup with 13 procedures. Our qualitative analysis demonstrates that even the minimal 0.5% concentration was sufficient to delineate the tumor itself, however in cases of multiple lesions localized in more than one liver

segments the concentrations below 5.0% were insufficient to reliably depict all tumor masses. The contrast agent concentrations of 0.5%, 1.0%, 1.5%, 2.5% and 3.0% were seldom rated as those of acceptable quality (see **Table 24** and **25**). Surprisingly, the concentration of 10.0% was not the best one either due to lack of contrast between the enhanced tumor and liver segment. The limitation of this analysis was the low number of procedures in this subgroup. Another issue is the different tumor morphology in the examined 9 patients; not every concentration was tested in all different tumor types. Nonetheless, we judged a concentration of 5.0% Gd-DOTA to be ideal for further studies of hepatic artery perfusion, since it demonstrated a superior quality. As expected, no catheter artifacts were observed in any of the used sequences since all inserted catheters were tested in our previous experiments.

Quantitative analysis

Quantitative analysis was performed in a second group of 18 patients with 49 TACE procedures. In all cases 5.0% concentration of the contrast agent was applied in three phases: arterial, portalvenous and late venous phase. It is disputable if the portalvenous phase in our study corresponds to the regular portal venous phase acquired after i.v. contrast agent injection. The acquisition time in regular MR liver examination is approximately 60 - 70 s after i.v. injection. In our study the portal venous phase was acquired 30 - 40 s after i.a. application of contrast agent at the latest. However, in all cases the HCC typical washout (5, 34, 37, 52, 69) of contrast agent was observed. Three phases performed one after another allowed us to observe the tumor perfusion as a dynamic process.

The SNR in the region of maximal tumor enhancement as well the SNR of the whole lesion were significantly higher in the VIBE sequence in all perfusion phases compared to the FLASH sequence. Moreover the VIBE in contrast to FLASH 3D sequence preserves wide anatomic coverage of the organs of the upper abdomen, maintaining adequate spatial resolution at the same time. On the other hand, the acquisition time were longer for the VIBE

sequence compared to the FLASH 3D (approximately 18 vs.11 seconds), but still within the margin of an easy breathe hold for the patient. The SNR measured in the liver demonstrated significant differences showing a better signal for the VIBE sequence. Even native MR scans of the liver before contrast agent application demonstrated the higher signal intensity of the liver compared to FLASH 3D. This can be explained by general macroscopically higher signal intensity of the unenhanced liver tissue in patients with liver cirrhosis in VIBE sequences. No statistically relevant differences were found between the SNR in point of maximal tumor enhancement and in the whole tumor. Most of our patients underwent multiple TACE approaches so the lesion enhancement patterns varied between consecutive procedures.

Contrast to noise ratios defined as the difference between SNR of the tumor and SNR of the liver related to noise demonstrated no significant differences between FLASH 3D and VIBE sequences either. This was true for both SNR measurements in the region of maximal tumor enhancement and in the whole tumor. In our opinion this could be due to the relatively small sample number. Of note, small tumors (<3cm) in multifocal HCC demonstrated the tendency of homogenous enhancement in contrast to larger lesions where multiple local necrotic areas were observed. The so-called "pseudocapsule", which is characteristic for well-differentiated HCC (2 patients), was not included into the ROIs due to its very thin coating. The differences between lesions morphology in several patients could also have an influence on signal intensities.

All MR scans were performed in transverse plane in order to achieve the best lesion depiction and to save time. In none of the sequences artifacts of the catheter were observed. Usually, only the part of the catheter localized in the hepatic artery was depicted. The catheter was recognizable after contrast agent injection due to the high signal intensity along the shaft. This can be explained by positive contrast principle of the T1 shortening contrast agent. Of note, the visualization of the catheter hindered the quality in none of the acquired

images. In both sequences (VIBE and FLASH 3D) clear tumor delineation was possible in good resolution and quality.

Follow up and benefits of intraaterial MR angiography

The combination of MR imaging with interventional radiology procedures offers a unique possibility of therapy monitoring and treatment planning. As demonstrated in **Figures 23 - 25** the simultaneous tumor supply from left and right hepatic artery might impede the treatment, especially in tumors in watershed distributions. The DSA image however imitates complete tumor perfusion after injection of contrast agent via the left hepatic artery due to the nature of its projection technique. TACE performed *via* the left hepatic artery would cause incomplete tumor targeting. In other published studies, the primary catheter position had to be revised in 25% (46) and in 40% (74) of procedures. The three-dimensional image acquisition is thereby crucial in estimation of adequate catheter position. Newer X-ray techniques integrated into a fluoroscopy unit might be also able to overcome the disadvantage of a DSA projection technique.

In our investigation we changed the catheter position in order to better target the HCC only in 14% of procedures. Overall, 5 patients already had undergone previous TACE therapy before inclusion in the study. This factor might have led to an improved primary catheter position for optimal tumor targeting in these patients. On the other hand, atypical recruitment of collaterals from the phrenic artery for example might only occur after treatment of the primary arterial supply to the tumor. Properly performed imaging prior to the procedure (CT/MRI) represents a pivotal determinant for the outcome of TACE. This can yield the necessary anatomical information needed for correct positioning of the catheter. Identification of new lesions, which demonstrated, apart from i.a. contrast uptake, also washout phenomenon, is an advantage of i.a. MR imaging observed during our study. These lesions presented only contrast uptake in the arterial phase in the regular MR scan performed prior the TACE and were classified as dysplastic nodules. Overall, it was the case in four

procedures (taking both subgroups into account). Considering their imaging features after i.a. contrast agent application they might be classified as potential HCC. Perfusion morphology of detected additional lesions after i.a. application of contrast agent might be however different from the one after i.v. application. Previously mentioned washout may occur due to shunts between the HCC and normal liver parenchyma. Nonetheless, the detection of new lesions might alter further therapy and such newly detected tumors should be further classified with a short-term follow-up MRI scan. One explanation for the lack of detection during standard MRI is that lesions in an early stage might be detectable only after selective i.a. application of contrast agent due to their small size and the better contrast uptake. Dynamic perfusion changes like washout in the portalvenous or late venous phase are highly suggestive of additional HCC lesions despite the fact that the perfusion dynamic after i.a. application of gadolinium is not a well-established method in classification of HCC. The literature clearly states that non-invasive diagnostic criteria in cirrhotic patients are indeed based on four-phase multidetector CT or dynamic contrast enhanced MR scans, but after i.v. contrast media application (5, 34, 37, 53, 69). Typical hallmarks of HCC like arterial hyperenhancement and venous washout are regarded as determinants of this type of tumors only in lesions larger than 2 cm present in the cirrhotic liver. In lesions with diameter below 2 cm, the nodule showing arterial contrast uptake must not necessarily be a HCC (27). The prospective study by *Forner et al.* (27) evaluated recently the accuracy of contrast-enhanced ultrasound together with MRI and fine needle biopsy for the diagnosis of the nodules smaller than 2 cm in the cirrhotic livers. The authors stated that the HCC in these cases might be established without a biopsy when both techniques are consistent and conclusive. The sensitivity of such criteria was however only 33%, because absence of malignant hallmarks does not exclude malignancy (27). In such cases close surveillance is recommended and this should be adapted to small nodule detected after i.a. contrast media application as well. The detection of HCC suspected lesion was the case in four patients in our study; these lesions were seen in standard MR examination as well, but due to a lack of washout they

were not categorized as malignant. The first patient suffered primarily from well-differentiated HCC in watershed distribution in segment 4 of the liver. He was included in the study after his first selective TACE treatment. The suspected lesion was identified as unclear contrast enhancement in i.a. MR angiography in the segment 6, showed however no clear washout in the late phases. The lesion measured initially 1.7 cm and was treated with chemoembolizing agent since the second TACE. In the follow-up MR examination the lesion was still classified as dysplastic nodule of the same size since the washout phenomena were absent. The TACE treatment of the lesion was this time impossible due to heavy vessel spasms. The next follow-up MR examination demonstrated the lesion of 1.9 cm (0.2 cm size progress) but still no washout. In i.a. MR angiography washout was this time however readily visible and the lesion was also treated with chemotherapy. However the changes in perfusion seen over time could in theory also be due to treatment effects. In the next follow-up MR the washout was eventually visible and the lesion was classified as another HCC, the size however was this time even lesser than initially (1.3 cm) (**Figures 27-30**). Eventually, this patient became a liver transplantation. The second patient suffered from well distinguishable singular HCC in the segment 6 of the liver with 5 small (<1.2 cm) lesions disseminated in the right liver lobe, mostly in segments 5 and 6. They were classified in the baseline MR examinations with i.v. contrast agent administration as dysplastic nodules since they demonstrated only strong arterial enhancement and did not show any washout in the portalvenous phase. In our study during TACE they were not readily depicted in the DSA image, probably due to small size. After i.a. contrast agent administration in the MR angiography examination they were however easily identified, one of them demonstrated moreover a washout phenomenon. All lesions were under treatment due to non-selective application of chemotherapy into the right liver lobe. In the next follow-up MR examinations the same lesion classified previously as dysplastic nodule showed eventually a washout and was classified as HCC lesion. Size of the lesions was not progressive. It is unclear why the lesion demonstrated typical hallmarks after chemoembolizing treatment and therefore it remains disputable, if this lesion is a HCC.

The third patient suffered from the recurrent HCC in the right liver lobe after left hemihepatectomy. By the time she was included in the study she suffered from 6 HCC lesions with the typical washout phenomena described in regular follow-up MR examination (1 day before TACE treatment). By the time of i.a. MR angiography all 6 lesions were readily depicted with typical HCC hallmarks and one small 1 cm nodule with washout phenomena was additionally depicted in segment 8. In the follow-up examination (5 weeks after TACE) this particular lesion demonstrated the washout phenomena and strong suspicion of new HCC. All lesions in this particular case showed inhomogeneous response pattern and the newly formed HCC in segment 8 demonstrated no size progress during next follow-up examinations. The fourth patient suffered from singular HCC located subcapsular in segment 8 of the liver. One other lesion (<1 cm in segment 7) without washout was diagnosed and classified as dysplastic nodule in the baseline MR examination. The i.a. MR angiography demonstrated at least two already centrally necrotic lesions <1 cm (liver segment 7 and 6) with marginal contrast enhancement but no washout. In the follow-up examination in about 5 weeks the lesions showed washout, which was debatable due to their small size below 1 cm, washout was however readily visible in i.a. MR angiography. Yet in 3 months follow-up multiple new HCC satellites metastases or newly formed HCC lesions were detectable in both liver lobes. In this case despite the selective and non-selective application of the chemoembolizing agent to the liver, TACE was not a successful method of treatment. Second imaging technique (contrast enhanced CT or sonography) was not employed in any of the patients. Like described above i.a. MR angiography seems to be very sensitive in detecting small HCC lesions, even under 1 cm size, but the histopathological correlation is required.

Most of the patients qualified for multiple TACE therapy. Three patients involved in our study underwent four consecutive procedures. Two of the patients demonstrated decrease of SNR measured in the whole tumor, most certainly due to good tumor targeting and developed necrotic areas within the tumor as consequence of therapy. However, in one

patient with multifocal HCC in the right liver lobe this was not the case. His treatment response was not equal in every lesion. Revascularization in one HCC satellite lesion was observed every single time in control MRI after TACE despite multiple treatments while other lesions showed no perfusion, i.e., were necrotic. On the other hand the native CT scan performed after TACE demonstrated the proper lipiodol distribution in all HCC lesions. Another six patients included in the study underwent three consecutive procedures. In these cases SNR of the whole tumor either remained the same or demonstrated the decrease expected, due to ischemic tumor areas. It is interesting to observe that especially those patients without prior TACE treatment showed a clear decrease in SNR.

Limitations of combining DSA and MRI are the prolonged procedure time of about 35 minutes and relocation of the patients from angiography room, which may potentially pose an increased infection risk. Therefore, we had decided not to measure the MR perfusion in the targeted lesion right after completing TACE like other authors (46, 75). Indeed, the native CT scan as gold standard allowed evaluating the lipiodol distribution in the targeted liver segment one day after procedure. Recently evaluated cone beam CT employed during TACE demonstrates similar success rates compared to intraprocedurel MRI (70). Its pivotal advantage is better image resolution and demarcation of vessels as well as no need of moving the patient during the procedure. High radiation dose as well as difficulties in separation of stained (i.e., from previous TACE procedures) lipiodol in the tumor with the newly applied one are the disadvantages. Furthermore, no additional detection of unknown lesions has been reported by cone beam CT. Cone beam CT was at the beginning of the study not available in our institution.

In conclusion, i.a. liver tumor perfusion in magnetic resonance angiography during TACE is feasible and safe for the patients. This method allows the detection of incorrect catheter location so that the therapy position may be easily revised yielding a better therapy result. Moreover it might contribute to improved therapy outcome due to early diagnosis of new developed potentially malignant lesions.

VII. REFERENCES

1.   Bakker CJ, Hoogeveen RM, Weber J, van Vaals JJ, Viergever MA, Mali WP. (1996) Visualization of dedicated catheters using fast scanning techniques with potential for MR-guided vascular interventions. Magn Reson Med 36:816-20.

2.   Bakker CJ, Hoogeveen RM, Hurtak WF, van Vaals JJ, Viergever MA, Mali WP. (1997) MR-guided endovascular interventions: susceptibility-based catheter and near-real-time imaging technique. Radiology 202:273-6.

3.   Bartels ED, Brun GC, Gammeltoft A, Gjorup PA. (1954) Acute anuria following intravenous pyelography in a patient with myelomatosis. Acta Med Scand 150:297–302.

4.   Bell JA, Saikus CE, Ratnayaka K, Wu V, Sonmez M, Faranesh AZ, Colyer JH, Lederman RJ, Kocaturk O. (2012) A deflectable guiding catheter for real-time MRI-guided interventions. J Magn Reson Imaging 35:908-15.

5.   Bhartia B, Ward J, Guthrie JA, Robinson PJ. (2003) Hepatocellular carcinoma in cirrhotic livers: double-contrast thin-section MR imaging with pathologic correlation of explanted tissue. AJR Am J Roentgenol 180:577-84.

6.   Bray F, Jemal A, Grey N, Ferlay J, Forman D. (2012) Global cancer transitions according to the Human Development Index (2008-2030): a population-based study. Lancet Oncol 13:790-801.

7.   Brenner DJ, Shuryak I, Einstein AJ. (2011) Impact of reduced patient life expectancy on potential cancer risks from radiologic imaging. Radiology 261:193-98.

8.   Bruix J, Sherman M. (2011) Management of hepatocellular carcinoma: an update. Hepatology 53:1020-2.

9.   Bruix J, Sherman M; Practice Guidelines Committee, American Association for the Study of Liver Diseases. (2005) Management of hepatocellular carcinoma. Hepatology 42:1208-36.

10.   Bücker A, Neuerburg JM, Adam G, Schürmann K, Rasche V, van Vaals JJ, Molgaard-Nielsen A, Günther RW. (1998) Stent placement with real time MRI guidance: initial animal experiment experiences. Rofo 169:655-7.

11.   Buecker A, Spuentrup E, Ruebben A, Günther RW. (2002) Artifact-free in-stent lumen visualization by standard magnetic resonance angiography using a new metallic magnetic resonance imaging stent. Circulation 105:1772-5.

12.   Buecker A, Adam GB, Neuerburg JM, Kinzel S, Glowinski A, Schaeffter T, Rasche V, van Vaals JJ, Guenther RW. (2002) Simultaneous real-time visualization of the catheter tip and vascular anatomy for MR-guided PTA of iliac arteries in an animal model. J Magn Reson Imaging 16:201-8.

13.   Buecker A, Spuentrup E, Schmitz-Rode T, Kinzel S, Pfeffer J, Hohl C, van Vaals JJ, Günther RW. (2004) Use of a nonmetallic guide wire for magnetic resonance-guided coronary artery catheterization. Invest Radiol 39:656-60.

14.   Burrel M, Reig M, Forner A, Barrufet M, de Lope CR, Tremosini S, Ayuso C, Llovet JM, Real MI, Bruix J. (2012) Survival of patients with hepatocellular carcinoma treated by transarterial chemoembolisation (TACE) using Drug Eluting Beads. Implications for clinical practice and trial design. J Hepatol 56:1330-5.

15.   Cammà C, Schepis F, Orlando A, Albanese M, Shahied L, Trevisani F, Andreone P, Craxì A, Cottone M. (2002) Transarterial chemoembolization for unresectable hepatocellular carcinoma: meta-analysis of randomized controlled trials. Radiology 224:47-54.

16.   Compagnone G, Giampalma E, Domenichelli S, Renzulli M, Golfieri R. (2012) Calculation of conversion factors for effective dose for various interventional radiology procedures. Med Phys 39:2491-8.

17.   Debatin JF, Adam G. (Eds.) (1998) Interventional Magnetic Resonance Imaging. Heidelberg: Springer-Verlag, Berlin.

18. Dietrich O, Raya JG, Reeder SB, Reiser MF, Schoenberg SO. (2007) Measurement of signal-to-noise ratios in MR images: influence of multichannel coils, parallel imaging, and reconstruction filters. J Magn Reson Imaging 26:375-85.

19. Dubois, G. An overview of radon surveys in Europe. (2005) Report EUR 21892 EN.

20. Dumoulin CL, Souza SP, Darrow RD. (1993) Real-time position monitoring of invasive devices using magnetic resonance. Magn Reson Med 29:411-5.

21. EASL: European Association For The Study Of The Liver; EORTC: Organisation For Research And Treatment Of Cancer. (2012) EASL-EORTC clinical practice guidelines: management of hepatocellular carcinoma. J Hepatol 56:908-43.

22. Edelstein WA, Bottomley PA, Pfeifer LM. (1984) A signal-to-noise calibration procedure for NMR imaging systems. Med Phys 111:180-5.

23. Erlebacher JA, Cahill PT, Pannizzo F, Knowles RJ. (1986) Effect of magnetic resonance imaging on DDD pacemakers. Am J Cardiol 57:437-40.

24. El-Serag HB, Richardson PA, Everhart JE. (2001) The role of diabetes in hepatocellular carcinoma: a case-control study among United States Veterans. Am J Gastroenterol 96:2462-7.

25. Ferlay J, Shin HR, Bray F, Forman D, Mathers C, Parkin DM. (2010) Estimates of worldwide burden of cancer in: GLOBOCAN 2008. Int J Cancer 127:2893-917.

26. Fischer W, Lampadius MS, Mols R, Schaefers G. (2013) MRT bei aktiven Implantaten: Generelle Sicherheit gibt es nicht. Dtsch Arztebl 110: A-555 / B-494 / C-494.

27. Forner A, Vilana R, Ayuso C, Bianchi L, Solé M, Ayuso JR, Boix L, Sala M, Varela M, Llovet JM, Brú C, Bruix J. (2008) Diagnosis of hepatic nodules 20 mm or smaller in cirrhosis: Prospective validation of the noninvasive diagnostic criteria for hepatocellular carcinoma. Hepatology 47:97-104.

28. Frericks BB, Elgort DR, Hillenbrand C, Duerk JL, Lewin JS, Wacker FK. (2009) Magnetic resonance imaging-guided renal artery stent placement in a Swine model: comparison of two tracking techniques. Acta Radiol 50:21-7.

29.   Gaba RC, Wang D, Lewandowski RJ, Ryu RK, Sato KT, Kulik LM, Mulcahy MF, Larson AC, Salem R, Omary RA. (2008) Four-dimensional transcatheter intraarterial perfusion MR imaging for monitoring chemoembolization of hepatocellular carcinoma: preliminary results. J Vasc Interv Radiol 19:1589-95.

30.   Glowinski A, Adam G, Bücker A, Neuerburg J, van Vaals JJ, Günther RW. (1997) Catheter visualization using locally induced, actively controlled field inhomogeneities. Magn Reson Med 38:253-8.

31.   Griswold MA, Jakob PM, Heidemann RM, Nittka M, Jellus V, Wang J, Kiefer B, Haase A. (2002) Generalized autocalibrating partially parallel acquisitions (GRAPPA). Magn Reson Med 476:1202-10.

32.   Haase A, Frahm J, Matthaei D, Hänicke W, Merboldt KD. (1986) FLASH imaging: rapid NMR imaging using low flip-angle pulses. J Magn Reson 213:533-41.

33.   Hallén E. (1962) Electromagnetic theory. Chapman-Hall, London.

34.   Hayashi M, Matsui O, Ueda K, Kawamori Y, Gabata T, Kadoya M. (2002) Progression to hypervascular hepatocellular carcinoma: correlation with intranodular blood supply evaluated with CT during intra-arterial injection of contrast material. Radiology 225:143-9.

35.   Hayes DL, Holmes DR Jr, Gray JE. (1987) Effect of 1.5 tesla nuclear magnetic resonance imaging scanner on implanted permanent pacemakers. J Am Coll Cardiol 10:782-6.

36.   Henkelman RM. (1985) Measurement of signal intensities in the presence of noise in MR images. Med Phys 12:232-3.

37.   Ito K, Fujita T, Shimizu A, Koike S, Sasaki K, Matsunaga N, Hibino S, Yuhara M. (2004) Multiarterial phase dynamic MRI of small early enhancing hepatic lesions in cirrhosis or chronic hepatitis: differentiating between hypervascular hepatocellular carcinomas and pseudolesions. AJR Am J Roentgenol 183:699-705.

38.   Kahlert P, Parohl N, Albert J, Schäfer L, Reinhardt R, Kaiser GM, McDougall I, Decker B, Plicht B, Erbel R, Eggebrecht H, Ladd ME, Quick HH. (2012) Real-time magnetic

resonance imaging-guided transarterial aortic valve implantation: in vivo evaluation in swine. J Am Coll Cardiol 59:192-3.

39.   Kellman P, McVeigh ER. (2005) Image reconstruction in SNR units: a general method for SNR measurement. Magn Reson Med 54:1439-47.

40.   Kos S, Huegli R, Hofmann E, Quick HH, Kuehl H, Aker S, Kaiser GM, Borm PJ, Jacob AL, Bilecen D. (2009) First magnetic resonance imaging-guided aortic stenting and cava filter placement using a polyetheretherketone-based magnetic resonance imaging-compatible guidewire in swine: proof of concept. Cardiovasc Intervent Radiol 32:514-21.

41.   Kos S, Huegli R, Hofmann E, Quick HH, Kuehl H, Aker S, Kaiser GM, Borm PJ, Jacob AL, Bilecen D. (2009) Feasibility of real-time magnetic resonance-guided angioplasty and stenting of renal arteries in vitro and in Swine, using a new polyetheretherketone-based magnetic resonance-compatible guidewire. Invest Radiol 44:234-41.

42.   Konings MK, Bartels LW, Smits HF, Bakker CJ. (2002) Heating around intravascular guidewires by resonating RF waves. J Magn Reson Imaging 12:79-85.

43.   Kraemer NA, Immel E, Donker HC, Melzer A, Ocklenburg C, Guenther RW, Buecker A, Krombach GA, Spuentrup E. (2011) Evaluation of an active vena cava filter for MR imaging in a swine model. Radiology 258:446-54.

44.   Krueger JJ, Ewert P, Yilmaz S, Gelernter D, Peters B, Pietzner K, Bornstedt A, Schnackenburg B, Abdul-Khaliq H, Fleck E, Nagel E, Berger F, Kuehne T. (2006) Magnetic resonance imaging-guided balloon angioplasty of coarctation of the aorta: a pilot study. Circulation 113:1093-100.

45.   Langen HJ, Kugel H, Heindel W, Krahe T, Gieseke J, Lackner K. (1997) Localization of puncture needles in MRI: experimental studies on precision using spin-echo sequences at 1.0 T. Rofo 167:501-8.

46.   Lewandowski RJ, Tepper J, Wang D, Ibrahim S, Miller FH, Kulik L, Mulcahy M, Ryu RK, Sato K, Larson AC, Salem R, Omary RA. (2008) MR imaging perfusion mismatch: a

technique to verify successful targeting of liver tumors during transcatheter arterial chemoembolization. J Vasc Interv Radiol 19:698-705.

47.   Lewin JS, Duerk JL, Jain VR, Petersilge CA, Chao CP, Haaga JR. (1996) Needle localization in MR-guided biopsy and aspiration: effects of field strength, sequence design, and magnetic field orientation. AJR Am J Roentgenol 166:1337-45.

48.   Liu CY, Farahani K, Lu DS, Duckwiler G, Oppelt A. (2000) Safety of MRI-guided endovascular guidewire applications. J Magn Reson Imaging 12:75-8.

49.   Llovet JM, Bruix J. (2003) Systematic review of randomized trials for unresectable hepatocellular carcinoma: Chemoembolization improves survival. Hepatology 37:429-42.

50.   Llovet JM, Di Bisceglie AM, Bruix J, Kramer BS, Lencioni R, Zhu AX, Sherman M, Schwartz M, Lotze M, Talwalkar J, Gores GJ; Panel of Experts in HCC-Design Clinical Trials. (2008) Design and endpoints of clinical trials in hepatocellular carcinoma. J Natl Cancer Inst 100:698-711.

51.   Marrero JA, Fontana RJ, Fu S, Conjeevaram HS, Su GL, Lok AS. (2005) Alcohol, tobacco and obesity are synergistic risk factors for hepatocellular carcinoma. J Hepatol 42:218-24.

52.   Morana G, Grazioli L, Kirchin MA, Bondioni MP, Faccioli N, Guarise A, Schneider G. (2011) Solid hypervascular liver lesions: accurate identification of true benign lesions on enhanced dynamic and hepatobiliary phase magnetic resonance imaging after gadobenate dimeglumine administration. Invest Radiol 46:225-39.

53.   McEvoy J, McGeown MG, Kumar R. (1970) Renal failure after radiological contrast media. Br Med J 19:717-8.

54.   McVeigh ER, Henkelman RM, Bronskill MJ. (1985) Noise and filtration in magnetic resonance imaging. Med Phys 12:586-91.

55.   Niendorf HP, Haustein J, Cornelius I, Alhassan A, Clauss W. (1991) Safety of gadolinium-DTPA: extended clinical experience. Magn Reson Med 22:222-8.

56.   Nitz WR, Oppelt A, Renz W, Manke C, Lenhart M, Link J. (2001) On the heating of linear conductive structures as guidewires and catheters in interventional MRI. J Magn Reson Imaging 13:105-14.

57.   Nitz R, Runge VM, Schmeets SH.(Eds.) (2007) Grundlagen der Bildgebung.CNR-Kontrast-Rausch-Verhaeltnis. Praxiskurs MRT. 2nd ed. Georg Thieme, Stuttgart.

58.   Parfrey PS, Griffiths SM, Barrett BJ, Paul MD, Genge M, Withers J, Farid N, McManamon PJ. (1989) Contrast material-induced renal failure in patients with diabetes mellitus, renal insufficiency, or both. A prospective controlled study. N Engl J Med 19:143-9.

59.   Pearce MS, Salotti JA, Little MP, McHugh K, Lee C, Kim KP, Howe NL, Ronckers CM, Rajaraman P, Sir Craft AW, Parker L, Berrington de González A. (2012) Radiation exposure from CT scans in childhood and subsequent risk of leukaemia and brain tumours: a retrospective cohort study. Lancet 380:499-505.

60.   Port JD, Pomper MG. (2000) Quantification and minimization of magnetic susceptibility artifacts on GRE images. J Comput Assist Tomogr 24:958-64.

61.   Pruessmann KP, Weiger M, Scheidegger MB, Boesiger P. (1999) SENSE: sensitivity encoding for fast MRI. Magn Reson Med 42:952-62.

62.   Reeder SB, Wintersperger BJ, Dietrich O, Lanz T, Greiser A, Reiser MF, Glazer GM, Schoenberg SO. (2005) Practical approaches to the evaluation of signal-to-noise ratio performance with parallel imaging: application with cardiac imaging and a 32-channel cardiac coil. Magn Reson Med 54:748-54.

63.   Riederer SJ, Tasciyan T, Farzaneh F, Lee JN, Wright RC, Herfkens RJ. (1988) MR fluoroscopy: technical feasibility. Magn Reson Med 8:1-15.

64.   Sangiovanni A, Prati GM, Fasani P, Ronchi G, Romeo R, Manini M, Del Ninno E, Morabito A, Colombo M. (2006) The natural history of compensated cirrhosis due to hepatitis C virus: A 17-year cohort study of 214 patients. Hepatology 43:1303-10.

65.   Scheffler K, Lehnhardt S. (2003) Principles and applications of balanced SSFP techniques. Eur Radiol 13:2409-18.

66.   Schenck JF, Jolesz FA, Roemer PB, Cline HE, Lorensen WE, Kikinis R, Silverman SG, Hardy C, Barber WD and Laskaris ET (1995) Superconducting open-configuration MR imaging system for image-guided therapy. Radiology 195:805-14.

67.   Schönberg, Stefan O.; Dietrich, Olaf; Reiser, Maximilian F (Eds.) (2007) Measurement of Signal-to-Noise Ratio and Parallel Imaging. Parallel Imaging in Clinical MR Applications 1st ed. Springer, Berlin, Germany.

68.   Takayasu K, Arii S, Ikai I, Omata M, Okita K, Ichida T, Matsuyama Y, Nakanuma Y, Kojiro M, Makuuchi M, Yamaoka Y; Liver Cancer Study Group of Japan. (2006) Prospective cohort study of transarterial chemoembolization for unresectable hepatocellular carcinoma in 8510 patients. Gastroenterology 131:461-9

69.   Taouli B, Losada M, Holland A, Krinsky G. (2004) Magnetic resonance imaging of hepatocellular carcinoma. Gastroenterology 127:144-52

70.   Tognolini A, Louie JD, Hwang GL, Hofmann LV, Sze DY, Kothary N. (2010) Utility of C-arm CT in patients with hepatocellular carcinoma undergoing transhepatic arterial chemoembolization. J Vasc Interv Radiol 21:339-47.

71.   Trichopoulos D, Bamia C, Lagiou P, Fedirko V, Trepo E, Jenab M, Pischon T, Nöthlings U, Overved K, Tjønneland A, Outzen M, Clavel-Chapelon F, Kaaks R, Lukanova A, Boeing H, Aleksandrova K, Benetou V, Zylis D, Palli D, Pala V, Panico S, Tumino R, Sacerdote C, Bueno-De-Mesquita HB, Van Kranen HJ, Peeters PH, Lund E, Quirós JR, González CA, Sanchez Perez MJ, Navarro C, Dorronsoro M, Barricarte A, Lindkvist B, Regnér S, Werner M, Hallmans G, Khaw KT, Wareham N, Key T, Romieu I, Chuang SC, Murphy N, Boffetta P, Trichopoulou A, Riboli E. (2011) Hepatocellular carcinoma risk factors and disease burden in a European cohort: a nested case-control study. J Natl Cancer Inst 103:1686-95.

72.   Tzifa A, Krombach GA, Krämer N, Krüger S, Schütte A, von Walter M, Schaeffter T, Qureshi S, Krasemann T, Rosenthal E, Schwartz CA, Varma G, Buhl A, Kohlmeier A, Bücker A, Günther RW, Razavi R. (2010) Magnetic resonance-guided cardiac interventions using

magnetic resonance-compatible devices: a preclinical study and first-in-man congenital interventions. Circ Cardiovasc Interv 3:585-92.

73.   Unal O, Korosec FR, Frayne R, Strother CM, Mistretta CA. (1998) A rapid 2D time-resolved variable-rate k-space sampling MR technique for passive catheter tracking during endovascular procedures. Magn Reson Med 40:356-62.

74.   Vogl TJ, Balzer JO, Mack MG, Bett G, Oppelt A. (2002) Hybrid MR interventional imaging system: combined MR and angiography suites with single interactive table. Feasibility study in vascular liver tumor procedures. Eur Radiol 12:1394-400.

75.   Wang D, Jin B, Lewandowski RJ, Ryu RK, Sato KT, Mulcahy MF, Kulik LM, Miller FH, Salem R, Li D, Omary RA, Larson AC. (2010) Quantitative 4D transcatheter intraarterial perfusion MRI for monitoring chemoembolization of hepatocellular carcinoma. J Magn Reson Imaging 31:1106-16.

76.   Yeung CJ, Susil RC, Atalar E. (2002) RF safety of wires in interventional MRI: using a safety index. Magn Reson Med 47:187-93.

VIII. RELATED PUBLICATIONS

Papers:

1. Heating and safety of a new MR compatible guidewire prototype versus standard nitinol guidewire. **Malgorzata Wolska-Krawczyk**, Martin A. Rube, Erwin Immel, Andreas Melzer and Arno Buecker. **(in press) accepted for publication in Radiological Physics and Technology, 2013**.

Book chapters:

1. Workflow Analysis, Design Modeling and Simulation for the Multimodality Imaging Operating System (MITOS). Fabiola Fernández-Gutiérrez, Graeme Houston, Jakob Elle Ole, **Malgorzata Wolska-Krawczyk**, Marek Orban, Andreas Melzer. Intraoperative Imaging and Image-Guided Therapy, Ed. Jolesz FA, New York, Springer Science + Business, **(in press), 2014.**

Oral presentations:

1. Prototype of MR compatible guidewire versus nitinol based guidewire in a saline filled phantom. A comparison of RF heating in 1.5 MR scanner. **Malgorzata Wolska-Krawczyk**, Martin Rube, Erwin Immel, Rachel J. Toomey, Fabiola Fernández-Gutiérrez, Arno Buecker, Andreas Melzer. 23rd Conference of the Society for Medical Innovation and Technology (SMIT), 2011,Tel-Aviv, Israel.

2. Semi-Active Resonant Markers for Interventional Device Localization in Phantom Experiments and in a Thiel Embalmed Cadaver Model in 1.5T Real-Time MR Imaging. Martin Alexander Rube, Erwin Immel, Rachel Toomey, **Malgorzata Wolska-Krawczyk**, Andreas Melzer. 23rd Conference of the Society for Medical Innovation and Technology (SMIT), 2011, Tel-Aviv, Israel.

3. Transcatheter-intraarterial magnetic resonance angiography (TI-MRA) for accurate guidance of transarterial chemoembolization (TACE) in patients with HCC. **Malgorzata Wolska-Krawczyk**, Alexander Massmann, Peter Fries, Roland Seidel, Guenter Karl

Schneider, Arno Buecker. 40 Jubilee Congress of Polish Medical Society of Radiology, 2013, Wroclaw, Poland.

Poster presentations:

1. Transcatheter intraarterial MR angiography for accurate guidance of TACE in patients with HCC. Alexander Massmann, **Malgorzata Wolska-Krawczyk**, Peter Fries, Roland Seidel, Guenter Karl Schneider, Arno Buecker. European Congress of Radiology (ECR), 2013, Vienna, Austria.

2. Measurements of excessive heating by resonating waves of nitinol based guidewire in a saline filled phantom and in a vessel of a Thiel embalmed human cadaver with artificially induced saline flow in a 1,5 Tesla MR scanner. **Malgorzata Wolska-Krawczyk**, Martin Rube, Erwin Immel, Rachel J. Toomey, Fabiola Fernández-Gutiérrez, Arno Buecker, Andreas Melzer. 23rd Conference of the Society for Medical Innovation and Technology (SMIT), 2011, Tel-Aviv, Israel.

3. Computer simulation for ergonomics and workflow improvement in multi-modal image-guidedinterventions: a new approach. Fabiola Fernández-Gutiérrez , Rachel Toomey, Graeme Houston, **Malgorzata Wolska-Krawczyk**, Ole Jakob Elle, Arno Buecker, Andreas Melzer. 23rd Conference of the Society for Medical Innovation and Technology (SMIT), 2011, Tel-Aviv, Israel.

4. Simulating the Imaging Operating Suite of the future. From angiography to multi-modal image-guidance: framework and pilot models. Fabiola Fernández-Gutiérrez F, Graeme Houston, **Malgorzata Wolska-Krawczyk**, Ole Jakob Elle, Arno Buecker, Andreas Melzer. 4th NCIGT and NIH Image Guided Therapy Workshop, 2011, Arlington, Virginia, United States.

IX. ACKNOWLEDGEMENTS

Curriculum Vitae wurde aus datenschutzrechtlichen Gründen nicht enthalten.

Tag der Promotion: 03.07.2014

Dekan: Prof. Dr. Michael D. Menger

Berichterstatter: Prof.Dr. Arno Bücker

Zweiter Berichterstatter: Prof. Dr. Frank Lammert